ACS Catalysis



pubs.acs.org/acscatalysis
Perspective

# Structural Dynamics of Metalloproteins and Redox Enzymology with Mix-and-Inject Time-Resolved Serial Femtosecond Crystallography

Faisal H. M. Koua,* Huijong Han, and Richard Bean

Cite This: ACS Catal. 2024, 14, 10853−10870
Read Online

ACCESS | Metrics & More | Article Recommendations

**ABSTRACT:** Time-resolved serial femtosecond crystallography (*tr*-SFX) enables the study of biomolecules in action at room temperature, thus facilitating the construction of *in crystallo* mini-3D biomolecular series (a stop-motion series) of biochemical reactions with unprecedented spatiotemporal details. One of the challenges encountered in expanding this method is the insufficient tools available for triggering the biomacromolecular reaction. Here, we highlight recent advances and challenges in the mix-and-inject (diffusion-based) *tr*-SFX (MISC) as a promising triggering method for studying the structural dynamics of metalloproteins, redox enzymes, and their reaction kinetics. We further discuss the results obtained using MISC *tr*-SFX and propose complex MISC (cMISC) as a tool to study complex reaction kinetics such as theenzyme-catalyzed bisubstrate (sequential and ping-pong) reactions.

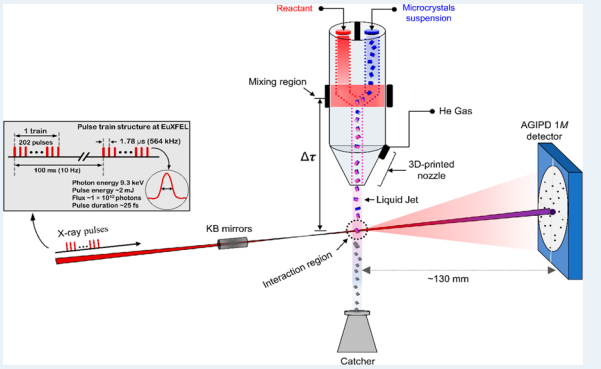


**KEYWORDS:** *biocatalysis, metalloproteins, redox enzymology, mix-and-inject tr-SFX, in crystallo enzyme kinetics, structural dynamics*



## INTRODUCTION

The extremely bright femtosecond X-ray pulses produced by X-ray free electron laser (XFEL) sources have revolutionized the field of structural biology and materials science with unprecedented capabilities for tracking the structure and dynamics of molecules in real time with high precision.[1−5] In particular, by using the diffraction-before-destruction concept,[1,6] this approach enables the study of inherently radiation-sensitive and scientifically challenging biological systems, such as metalloproteins and redox metalloenzymes, soluble and membrane-embedded proteins, such as photosystem II, cytochrome *c* oxidase, ferredoxins, hydrogenases, and heme peroxidases.[7−14] X-ray diffraction studies on metalloproteins are particularly challenging in conventional macromolecular crystallography owing to radiation damage. The damage is caused primarily by high-flux X-ray exposure over time scales ranging from milliseconds to seconds, which is longer than the photon ionization processes. Consequently, this extended exposure leads to significant damage to the unit cells of the crystals even at cryogenic temperatures, and this damage becomes more severe at room temperature.[15−23]

At synchrotron X-ray sources, photoionization of metal ions with high atomic numbers ($Z$) due to X-ray irradiation is unavoidable and may reach a very high reduction rate, even when collecting diffraction data at cryogenic temperatures with much lower X-ray doses.[7,8,15,17,23,24] There are two types of damage: *i*) global damage, which mostly affects the Bragg peak intensities and high-angle reflections; and *ii*) local damage, which occurs in the form of chemical deformations in specific regions of biomacromolecules, such as metal centers, disulfide bonds, and specific regions of residues.[12,21,25,26] Damage may occur indirectly in the metal centers of metalloproteins due to the high tendency of large Z atoms to absorb free electrons generated by X-ray irradiation and change their oxidation states. This, in many cases, results in a misleading interpretation of biological function.[17,20,27,28] This is particularly evident when insufficient care is taken during data collection and during the analysis of metalloproteins and redox enzymes.[29,30] These challenges are extended further when dealing with biological samples that are difficult to purify and crystallize, such as membrane proteins, adding another dimension to the above-mentioned complexity.

The ultrashort pulses of X-rays at XFELs, i.e., in the femtosecond regime, provide unprecedented opportunities for structural biologists to overcome the inherent challenges posed by X-ray radiation damage by collecting diffraction images before the onset of radiation damage.[2−5,21,31−33] One of these challenges is the study of redox reactions catalyzed by metalloproteins (redox enzymology), which involve redox

Received: April 28, 2024
Accepted: June 24, 2024
Published: July 4, 2024

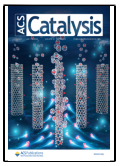

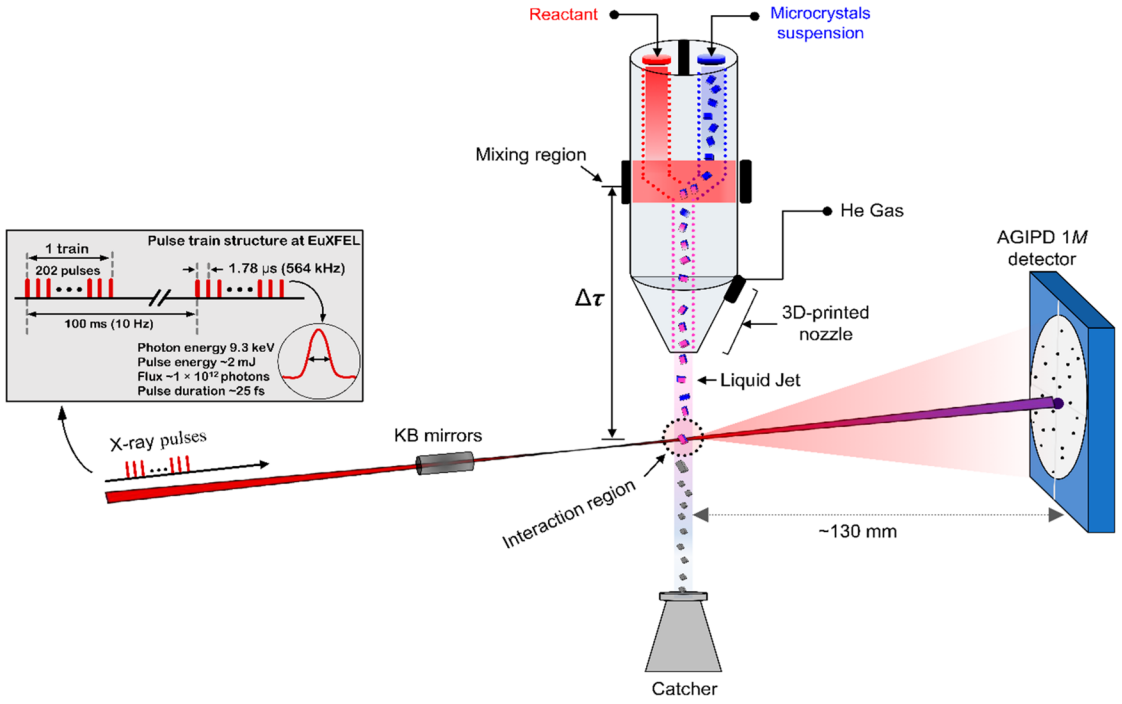


**Figure 1.** Schematic representation of the typical mix-and-inject *tr*-SFX experimental setup at the SPB/SFX instrument of the European XFEL [for example, see ref 41]. In MISC experiments, micrometer-sized crystals (with defined dimensions) are mixed with a substrate on the fly starting in the mixing injector, and the microcrystals are then probed with ~25 fs pulses of an X-ray-free electron laser at several delay times. The delay times ($\Delta t$) can be controlled by either the loop of the mixing injector or by changing the distance between the interaction point and the mixing starting point in the mixer, as indicated in the figure with a vertical double-headed arrow. The European XFEL delivers X-rays in pulse trains at 10 Hz, where each train consists of up to 2700 pulses with an intratrain repetition rate of 4.5 MHz.[36,38] The SPB/SFX instrument operates at up to a 1.13 MHz intratrain repetition rate with up to 352 pulses per train, ensuring sufficient data sets in a very short time, which is necessary for time-resolved experiments and enables the collection of sufficient data per delay time, thereby reducing the time required to complete the MISC *tr*-SFX experiments without compromising the data quality. With the SPB/SFX instrument, two sets of focusing Kirkpatrick-Baez (KB) mirrors can be used for SFX data collection from micron-focused (~2 $\mu$m) or nanofocused beams (~300 nm) with tunable photon energies usually at 9.3 keV (~1.33 Å) or 12.4 keV (~1.0 Å) up to ~16 keV. Various types of 3D-printed mixing injectors are available for MISC *tr*-SFX experiments,[42] and the instrument is also suitable for other types of mixing injectors, including a drop-on-demand injector.[37,147] With the SPB/SFX instrument, the MISC *tr*-SFX data are collected on an adaptive gain-integrating pixel detector (AGIPD) that was developed specifically to meet the unique high X-ray pulse repetition rates of the European XFEL. The instrument also uses a direct beam (focused on compound refractive lenses) in a downstream interaction region operated at a 10 Hz rate on a Jungfrau 4M detector, a 2D charge-integrating pixel detector developed by the Paul Scherrer Institute,[186] which is suitable for high-viscosity extruders (HVEs), including mixing-HVEs for the study of membrane proteins and their reaction dynamics at slower rates up to 40 s of mixing delay.

cofactors and residues susceptible to photoreduction, such as heme metal centers in hemoproteins and metal clusters in iron−sulfur proteins and nitrogenases.[22,34,35] Here, we highlight recent advances and challenges in studying the structural dynamics of metalloproteins and redox enzymology using the mix-and-inject time-resolved serial femtosecond crystallography (MISC) method. We also discuss the unique high repetition rate X-ray pulse structure of the European X-ray Free Electron Laser facility[36−38] and its importance in the study of complex and vulnerable biological macromolecules that are highly prone to X-ray radiation damage, such as redox-induced structural changes during the catalysis of metalloenzymes. These studies often require a large amount of experimental data to be collected to cover the complete reaction cycle of the process under investigation; notably, obtaining beamtime to conduct such experiments is extremely competitive with the limited number of XFEL facilities worldwide. A general schematic representation of the MISC experiments performed with the Single Particles, Clusters, and Biomolecules & Serial Femtosecond Crystallography (SPB/SFX) instrument of the European XFEL is shown in Figure 1 (see refs 36−40 for the detailed instrumentation and experimental setup).

## STRUCTURAL DYNAMICS OF METALLOPROTEINS AND REDOX ENZYMOLOGY

## DYNAMICS OF METALLOPROTEINS

Metalloproteins are a large group of proteins in which one or more metal ions are bound at specific sites in the protein. These proteins are ubiquitous in biological systems, and half of all proteins are estimated to contain regulatory (e.g., $Ca^{2+}$ in cellular signaling), catalytic (e.g., $Mn^{3+/4+}$ in the $Mn_4O_5Ca$ cluster of photosystem II), or structural metal ions (e.g., $Zn^{2+}$, such as in the Zn-finger) that are essential for their function.[22,29,43] The transition metals $Zn^{2+}$, $Mn^{2+,\ 3+,\ 4+}$, $Co^{2+,\ 3+}$, $Mo^{2+,\ 3+,\ 4+,\ 5+,\ 6+}$, and $Cu^{+,\ 2+}$ and $Fe^{2+,\ 3+,\ 4+}$ are among the most abundant metals in proteins. They have characteristic d-electrons, enabling the formation of discrete metal complexes in proteins where ligands are strongly bound via a range of coordination modes.[44] These transition metals are highly prone to X-ray radiation damage, which causes photoionization in the inner shells of the atom, which


https://doi.org/10.1021/acscatal.4c02526
ACS Catal. 2024, 14, 10853−10870

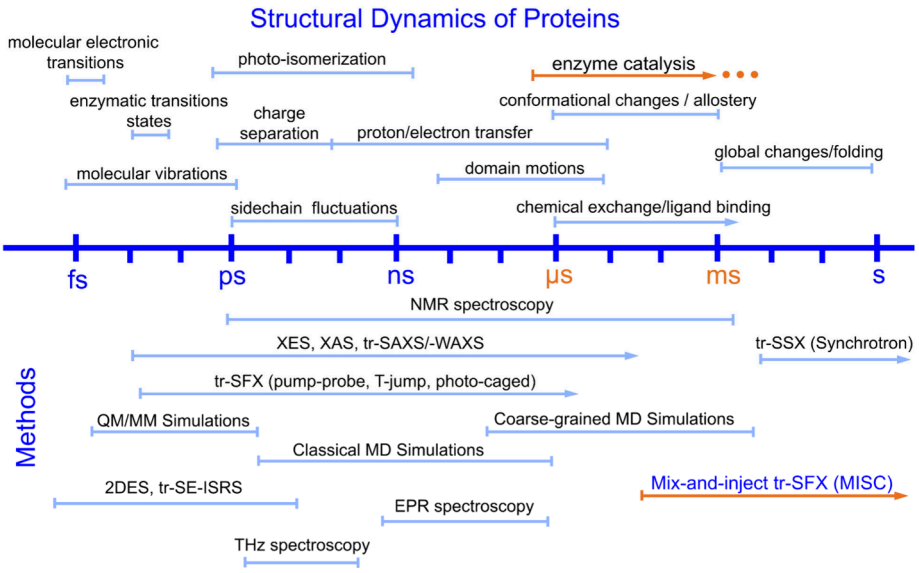


**Figure 2.** Time scales of the structural dynamics of proteins and methods used to track them. Outlines of protein structural dynamics, time scales, and methods used to probe them. Different methods can be used to track protein dynamics at ultrafast time scales, such as molecular vibrations and enzyme transitions, which can be determined using, for instance, theoretical calculations such as quantum mechanisms and molecular mechanics (QM/MM) and ultrafast spectroscopy such as 2D electron spectroscopy (2DES) or pump−probe *tr*-SFX at the fs−ps time scale. For enzyme catalysis (highlighted in orange), including local conformational changes, allostery, chemical exchange, and ligand binding, which occur at $\mu$s-to-ms time scales, MISC *tr*-SFX complemented with first-principles calculations, such as coarse-grained MD simulations, remains the method of choice. XES, X-ray emission spectroscopy; XAS, X-ray absorption spectroscopy; *tr*-SAXS/-WAXS, time-resolved small- and wide-angle X-ray scattering; T-jump, temperature jump; *tr*-SE-ISRS, time-resolved surface-enhanced impulsive stimulated Raman spectroscopy.

eventually leads to their reduction, thereby altering their biological oxidation state. This phenomenon is particularly devastating for redox proteins, as it alters the biochemical function of the protein, thereby misleading data interpretation in most cases.[17,45]

Many examples of metalloproteins, including those involved in photosynthesis, cellular respiration, redox homeostasis, and oxidative-stress-related proteins, have been extensively studied using various biophysical methods. These methods include X-ray absorption spectroscopy, static and time-resolved crystallography, attenuated total reflectance-Fourier transform infrared spectroscopy (ATR-FTIR), FTIR difference spectroscopy, FTIR spectroelectrochemistry, neutron crystallography, and electron paramagnetic resonance spectroscopic techniques as well as theoretical methods.[7−9,15,18,21,33,46−71] These studies have shaped our understanding of these vital biological processes in significant detail. In particular, the advent of *tr*-SFX has opened new opportunities to resolve ultrafast biochemical processes with high spatiotemporal resolution, especially in metalloproteins. It enables the tracking of ultrafast processes such as energy, electron transfer, and redox tuning in catalysis without noticeable photoreduction in catalytic metals.[63,65−69]

Metalloproteins play essential roles in biological systems and are involved in crucial processes such as oxygen transport, electron transfer, removal of free radicals (e.g., nitric oxide and peroxides), and energy transduction.[30,70,72] Their functions depend mainly on the chemistry of the metal cofactors, their coordination, and the protein environment of the metals.[73,74] Studying the conformational changes of these metalloproteins using the *tr*-SFX technique can significantly extend our understanding of these biological systems. This knowledge could eventually facilitate the optimal design of artificial catalysts, for instance, by mimicking the energy transfer process in photosystems to ultimately yield comparable efficiencies, thereby facilitating the transformation of this biomimicking technology to industrial scales.[59,75] A reliable biochemical understanding of the function or catalysis of these metalloproteins, i.e., metalloenzymes, can be achieved by collecting *tr*-SFX diffraction images before the propagation of radiation damage in the vicinity of metal cofactors using the so-called "short-pulse duration" (few femtoseconds) and, more importantly, enabling SFX data collection at near-physiological temperatures, thus allowing reliable interpretations of their biological functions. The feasibility of using *tr*-SFX for studying metalloproteins has been successfully demonstrated using a pump−probe approach in several systems that are light sensitive, including photosystems,[63,65−67,76] cytochrome *c* oxidases (*Cc*O),[77,78] cytochrome P450 NO reductase,[64] flavoenzymes such as DNA photolyases,[79] and various heme proteins.[80,81] Nonetheless, only a few of these studies have implemented diffusion-based *tr*-SFX to elaborate on the dynamics of metalloproteins or redox enzymes.[77,82−84]

## STRUCTURAL DYNAMICS IN REDOX ENZYMOLOGY

Redox reactions catalyzed by metalloproteins (i.e., metalloenzymes) can be traced using *tr*-SFX methods, ideally with a pump−probe technique. The pump−probe *tr*-SFX technique utilizes optical (pump) pulses to initiate biochemical reactions *in crystallo*, followed by X-ray FEL (probe) pulses to probe the reaction at different delay times. Consequently, light-triggered reactions can be visualized in real time with high temporal and spatial resolution.[18,31,21,39,85−95] The pump probe *tr*-SFX enables the determination of previously inaccessible reaction intermediates of light-induced processes such as photosynthetic light-induced water oxidation (Kok's cycle), molecular events of vision in mammals, the photocycle of DNA


https://doi.org/10.1021/acscatal.4c02526
ACS Catal. 2024, 14, 10853−10870

**Table 1. Summary of MISC *tr*-SFX and *tr*-SSX Method Development and the Structural Models Released in Recent Years**

| year | samples | PDB IDs | crystal dimension, μm, ligand/substrate | sample injection | diffusion method | XFEL/SR sources | delay times (Δ*t*), spatial resolutions | remarks | ref |
|---|---|---|---|---|---|---|---|---|---|
| 2017 | Riboswitches of *Vibrio vulnificus* | 5E54, 5SWD, 5SWE | 1−10 μm length to max. 20 μm, inhomogeneous | Viscous T-junction mixer connected to GDVN nozzle, 50 μm capillary | MISC *tr*-SFX | CXI instrument/LCLS: 9.2−9.5 keV XFEL energy (~$10^{11}$ photons), 50 fs length, 120 Hz repetition rate, 2−3 μm focal spot, CSPAD detector | 0 s (apo), 10 s, 10 min with 2.30−3.0 Å resolution | First reported MISC with XFEL at a slower reaction of riboswitches | 96 |
| 2017 | B-Lactamase (BlaC) of *M. tuberculosis* | Not released | ~3−10 × 3−10 × 2−3 $\mu m^3$ | Liquid T-junction mixer connected to GDVN nozzle | MISC *tr*-SFX | CXI Instrument/LCLS: 9 keV XFEL energy, 120 Hz, 40 fs length, CSPAD detector | 0 s (apo), 2 s with 2.8 and 2.4 Å resolution | ~5× improved temporal resolution enabled by using smaller crystals and liquid T-junction | 97 |
| 2018 | B-Lactamase (BlaC) of *M. tuberculosis* | 6B6B, 6B6C, 6B6F, 6B6D, 6B6E, 6B5X, 6B6A, 6B69, 6B5Y, 6B68 | 10 × 10 × 3 $\mu m^3$ (shards) and 5 × 2 × 2 $\mu m^3$ (needles), homogeneous | Mixing injector connected to GDVN nozzle | MISC *tr*-SFX | CXI Instrument/LCLS: 9.5 keV energy, 120 Hz repetition rate, data recorded on CSPAD detector | 0 s (apo), 2 s, 500, 100, and 30 ms, at 1.8−2.75 Å resolution | Milliseconds temporal resolution enabled by new type of mixer; sub-2 Å spatial resolution was achieved | 104 |
| 2019 | Bovine cytochrome *c* oxidase (C*c*O) | 6NKN, 6NMP, 6NMF | 20 × 20 × 4 $\mu m^3$ | Two-photon 3D printed hydrodynamic focusing mixer connected to GDVN nozzle | MISC *tr*-SFX | MFX Instrument/LCLS: 120 Hz repetition rate, 40 fs pulse length, CSPAD detector | 8 s at 2.5 Å resolution; 0 s (reduced-apo; oxidized-apo) at 2.8−2.8 Å | First ever structural trapping of the $P_R$-intermediate in C*c*O | 77 |
| | Isocyanide hydratase (ICH) from *Pseudomonas fluorescens* | 6NPQ, 6UND, 6UNF | 20 × 20 × 2 $\mu m^3$ | Co-MESH injector | MISC *tr*-SFX | MFX Instrument/LCLS: 9.5 keV (~$10^{12}$ photons), 40 fs at 30 Hz rate, 3 μm focus, Rayonix MX340-XFEL CCD detector | 0 s (apo), 15 s, and 5 min at 1.55 Å resolution | Visualizing previously hypothetical reaction mechanism on ICH | 83 |
| 2019 | HEWL and xylose isomerase | 6RNB, 6RNC, 6QNB, 6QNH, 6RND, 6RNF, 6QNC, 6QNI, 6QNJ, 6QND | 10 × 10 × 10 $\mu m^3$<br>10 × 10 × 20 $\mu m^3$<br>10 × 20 × 20 $\mu m^3$<br>20 × 20 × 20 $\mu m^3$<br>20 × 20 × 30 $\mu m^3$<br>20 × 25 × 25 $\mu m^3$<br>50 × 50 × 50 $\mu m^3$ | LAMA setup with Hamburg photochip solid target | LAMA *tr*-SSX | P14 and P14-2 beamlines/PETRA II (DESY): data collection on Eiger 4M, Eiger 16 M and Pilatus 2M detectors | 50 ms, 100 ms, 1.0 s (HEWL), 0 s (apo), 15 ms, 30 ms, 100 ms, 1.0, 4.5, and 60 s at 1.7−2.0 Å resolution | First application MICS using SR sources | 98 |
| 2021 | B-Lactamase (BlaC) of *M. tuberculosis* | 7K8L, 7K8E, 7K8F, 7K8H, 7K8K | 10 × 10 × 2 $\mu m^3$ | Mixing injector with a microfluidic holder connected with GDVN nozzle | MISC *tr*-SFX | SPB/SFX Instrument at EuXFEL: 9.3 keV, 40 fs pulse duration, 1.5 mJ pulse energy, 0.564 MHz repetition rate, data recorded with AGIPD detector under vacuum | 0 s (apo), 5 ms, 10 ms, 50 ms, 66 ms at 2.4−2.8 Å resolution | Attained the first single millisecond temporal resolution by the BlaC with Ceftriaxone antibiotic | 41 |
| | HEWL and CTX-M-15 β-lactamase | 7BHK, 7BHL, 7BHM, 7BHN, 7BH3, 7BH4, 7BH5, 7BH6, 7BH7 | Highly homogeneous<br>No information regarding the sizes of microcrystals, but the droplets were large enough to cover the crystals. Four nL crystals and 60 pL substrates | Drop-on-demand/drop-on-drop injection: An acoustic droplet ejection transducer with substrate depositor piezoelectric injector on Kapton tape | MISC *tr*-SFX and MISC *tr*-SSX | BL2/SACLA: 10 keV photon energy, 0.45 mJ, 10 fs pulse, 1.4 μm focus and 30 Hz rate, data recorded on a Rayonix MX300-HS detector.<br>I24 Beamline/DLS: 12.4 keV (5.2 × $10^{12}$ ph $s^{-1}$), 10 ms exposure time, 8 × 8 $\mu m^2$, data recorded on Pilatus 6M detector | 0 s (apo), 200 ms, 600 ms, 2 s, and 10 min at 1.45 to 1.65 Å resolution | Applying a drop-on-demand method for mixing experiments at XFEL and SR sources | 147 |



https://doi.org/10.1021/acscatal.4c02526
ACS Catal. 2024, 14, 10853−10870

**Table 1. continued**

| year | samples | PDB IDs | crystal dimension, $\mu$m, ligand/substrate | sample injection | diffusion method | XFEL/SR sources | delay times ($\Delta t$), spatial resolutions | remarks | ref |
|---|---|---|---|---|---|---|---|---|---|
| | Phospho-enol-pyruvate carboxykinase from rat | 7L36, 7L3M, 7L3V | $2 \times 2 \times 2$ $\mu m^3$ | Plunge cooler (a plunge-through-film) | Cryogenic Mix-and-Quench (MMQX) SSX | BL7B2/CHESS: 11 keV photon energy, $2 \times 10^{11}$ ph $s^{-1}$, $9 \times 12$ $\mu m^2$ focus, data collected on Pilatus 6M detector | 0 s (apo), 40 ms, and 120 ms at 1.84 to 2.07 Å resolution | Cryogenic *tr*-SSX enabled by fast mixing followed by cryo-cooling in LN2 | 189 |
| | | | $5 \times 5 \times 5$ $\mu m^3$ | | | | | | |
| | | | $10 \times 10 \times 10$ $\mu m^3$ | | | | | | |
| | | | $10 \times 20 \times 30$ $\mu m^3$ | | | | | | |
| | | | $20 \times 20 \times 20$ $\mu m^3$ | | | | | | |
| | | | $30 \times 30 \times 30$ $\mu m^3$ | | | | | | |
| | | | $40 \times 40 \times 40$ $\mu m^3$ | | | | | | |
| 2023 | B-Lactamase (BlaC) of *M. tuberculosis* | 8GCV, 8GCS, 8GCT, 8EBI, 8EBR, 8GCX, and 8ECF | $10 \times 10 \times 2$ $\mu m^3$ | Mixing injector with a microfluidic holder connected with GDVN nozzle | MISC *tr*-SFX | MFX Instrument/LCLS: 9.8 keV, 20−40 fs at 120 Hz rate, 3 $\mu$m focus, CSPAD detector | 0 s (apo), 3 ms, 6 ms, 15 ms, 240 ms, 700 ms, 3 h (soaking) at | The shortest delay times to be recorded for MISC experiment at 3 ms for BlaC bound to its inhibitor sulbactam | 105 |
| | | | Highly homogeneous | | | | | | |
| | Iq-mEmerald protein and GPCR | Not released | $5 \times 15$ $\mu$m | mixing-HVE injector | MISC *tr*-SFX | SPB/SFX instrument/EuXFEL: downstream interaction region, 12.4 keV, ∼ 2 mJ pulse, 100 fs length, 2 $\mu$m focus, CRLs focusing, in-helium environment, data recorded on Jungfrau 4M detector with 10 Hz rate | 0 s (apo), 18.5 s, 20 s, 30 s, 40 s | Demonstration of mixing in viscous LCP medium suitable for membrane proteins and slower reaction kinetics | 123 |
| 2023 | Cytochrome P450 CYP121 from *M. tuberculosis* | 8TDQ, 8TDP | Large crystals vortexed to microcrystals | Drop-on-demand rapid mixing method | MISC *tr*-SFX | LCLS: 9.3 keV photon energy, 30 Hz with 4 mJ or 2.2 mJ, 35 fs pulse length, 3 $\mu$m focus, data recorded on Rayonix MX340-HS detector | 0 s (ES), 200 ms at 1.65−1.85 Å resolution | First structural trapping of Cpd 0 hydroperoxo intermediate of cytochromes | 112 |
| | CTX-M-15 B-lactamase and Xylose isomerase | 8AWY, 8B3M, 8B2W, 8B2O, 8AWS, 8AWU, 8AWV, 8AWX, 8BO3, 8BO5, 8BO6, 8BO8 | $10 \times 15 \times 15$ $\mu m^3$ | LAMA setup with SPINE-standard sample holder (spitrobot) | LAMA *tr*-SSX (cryogenic) | MXCuBE/ESRF: 12.7 keV (∼$2 \times 10^{13}$ ph. $S^{1-}$), $7 \times 3$ $\mu$m focus, data collection on Eiger2 CdTe 16M detector | 0 s (apo), 50 ms, 250 ms, 500 ms, 1 s, 5 s | Wide scale *tr*-SSX for ligands binding over ms to s delay times | 148 |
| | | | $20 \times 20 \times 20$ $\mu m^3$ | | | | | | |
| 2024 | ICH from *Pseudomonas fluorescens* | 8VPW, 8VQ1 | $10 \times 10 \times 30$ $\mu m^3$ | Co-MESH injector | MISC *tr*-SFX | MFX Instrument/LCLS: 12 keV (∼$10^{12}$ photons), 40 fs at 120 Hz rate, 3 $\mu$m focus, Rayonix MX340-XFEL CCD | 0 s (apo), 30 s at 1.3 Å resolution | Trapping a long-range conformation upon substrate binding and intermediate formation | 84 |
| | HEWL, and pyridoxine synthase (Pdx1) from *Arabidopsis thaliana* | 8S2V, 8S2X | 3 $\mu$m, and 2 $\mu$m | Microfluidic droplets with subpicolitre scales | MISC *tr*-SSX | ID29 beamline/ESRF: 11.56 keV with 90 $\mu$s pulse, $2 \times 4$ $\mu m^2$ focus and 231.25 Hz rate, data recorded on Jungfrau 4M detector | <2 ms, 1.75 ms with dyes | Achieving delay times shorter than 2 ms. Currently the shortest mixing time to be achieved | 190 |



https://doi.org/10.1021/acscatal.4c02526
ACS Catal. 2024, 14, 10853−10870

repairs, and ion pumping in prokaryotes.[176−182] However, in nature, only a few proteins are photoactive, while the majority are nonphotoactive proteins. Therefore, methods for tracking the dynamics of nonphotoactive proteins must be developed to expand the utility of the *tr*-SFX tool. There are two alternative methods for triggering biochemical reactions in proteins: *i*) diffusion-based methods and *ii*) photocaged methods.[41,64,96−100] Both methods are promising for *tr*-SFX and synchrotron time-resolved serial crystallography (*tr*-SSX) for the study of nonphotoactive proteins; indeed, these methods have been implemented successfully,[64,96,97] as the former is the most realistic method because it uses natural sources that can be widely applied to trigger enzymatic reactions. This is achieved by direct and rapid mixing of protein nanocrystals with their substrate and probing the enzyme dynamics and reaction kinetics at different delay times.[100]

Protein dynamics play an important role in enzyme catalysis.[183,184] To this end, many methods have been developed to track the reaction-induced dynamics of enzymes and proteins in general (Figure 2). These methods rely mostly on the *in-solution* characterization of the proteins, which provided significant details on enzyme catalysis covering dynamics in a wide-range of temporal resolution from fs to s. On the other hand, time-resolved structural studies were only feasible with solid-state NMR for small proteins (MW ≤ 30 kDa) and time-resolved Laue diffraction on large crystals at synchrotrons, which laid the foundations in the field of time-resolved macromolecular crystallography. However, Laue diffraction is extremely sensitive to the degree of crystallinity, which is difficult to achieve due to the common high mosaic spread in protein crystals. The Laue method is limited to photoactivated biological reactions only including those activated with photocaged compounds. Moreover, the complexity of handling Laue spots, i.e., polychromatic rays of single to multiple reciprocal space reflection(s), has also contributed to the limited application of this method, which includes only a very narrow range of proteins. Most of these limitations have been overcome by the *tr*-SFX method, thus enabling a broader application of protein time-resolved crystallography. Nonetheless, direct structural observation of protein structural changes, especially for nonphotoactive proteins, has remained challenging until recently due to technical limitations, especially those related to sample delivery methods such as rapid mixing injectors. To improve the time scale to a single millisecond resolution and beyond, which is essential for tracking enzyme catalysis and dynamics, Pollack and co-workers developed a sophisticated mixing injector. This approach significantly improved the mixing time to reach a single millisecond resolution.[122] However, achieving uniform crystal sizes and subsequent rapid mixing of the substrate *in crystallo* for a precise delay time approximation across crystals remains highly challenging because the heterogeneity in reaction initiation may result in a mixture of different transient states at a single delay time. Recently, a droplet microfluidic device has been developed that enables precise control of the crystal sizes in subpicoliter droplets, thereby enhancing the rapid mixing of the substrate in the crystal with temporal resolution faster than 2 ms and up to 1.8 and 2.5 Å spatial resolutions for lysozyme and Pdx1 microcrystals after mixing with ligands (Table 1). This newly developed technology provides a sophisticated solution to some of the challenges in time-resolved serial crystallography in general. For example, the new device addresses the following challenges: (i) it excludes the need to handle microcrystals, thus reducing the differences between different batches and decreasing the variations in crystallographic statistics; (ii) it produces homogeneous microcrystals (∼2−3 $\mu$m) in highly monodispersed subpicolitre droplets, allowing rapid and uniform substrate diffusion with rates much faster than the lifetime of the reaction intermediates; and (iii) the method also reduces the need for a large amount of sample, as is the case for traditional mixing experiments with GDVN nozzles.[190] Rapid mixing in the droplets is initiated by impact-induced convection, thereby allowing fast and efficient mixing. The space between the droplets on the drop-on-demand Kapton tape can also be highly controlled, ensuring an accurate mixing time among droplets as well as transporting the mixture to the X-ray interaction region with a precise temporal resolution.[112,147,190] However, it remains challenging to apply this technology to high repetition rate XFEL facilities such as the European XFEL and the upcoming sources such as LCLS II and SHINE. Improving physical factors such as the Kapton speed, droplet velocity, crystal size, and concentration of ligands (diffusion time) will allow for faster reaction initiation as well as the rate at which the droplets reach the interaction region.

The MISC *tr*-SFX is suitable for the measurement of irreversible enzymatic reactions or other transient structures formed during irreversible biological/biochemical or chemical processes that cannot be measured using other methods, such as conventional X-ray crystallography or cryo-electron microscopy. Alterations in the crystalline structure due to irreversible conformational changes cannot be tracked in a single crystal or may require thousands of large crystals to achieve a complete data set for a single delay time, making this experiment impractical. On the other hand, the temporal resolution at third-generation synchrotrons is limited by the pulse length, which is in the millisecond range. This pulse length is also a limiting factor in metalloproteins, as longer pulse durations with high synchrotron radiation may cause serious damage to metalloenzymes. Therefore, MISC *tr*-SFX represents an ideal method for studying the structural enzymology of nonphotoactive enzymes. Table 1 summarizes recent studies using the MISC time-resolved crystallography method at both XFEL and synchrotron sources and the progress that has been made thus far to make the method more versatile.

The development of mixing devices has led to significant advances in the MISC *tr*-SFX method, as demonstrated by the study of the *Mycobacterium tuberculosis* ß-lactamase BlaC enzyme, a major determinant of ß-lactam antibiotic resistance,[101−103] in complex with third-generation cephalosporin antibiotics (ceftriaxone (CEF)) as well as the ß-lactamase inhibitor sulbactam.[41,97,104,105] The temporal resolution has improved drastically to 3−5 ms, opening up the potential for studying the structural dynamics of nonphotoactive enzymes. In these pioneering studies, Schmidt and co-workers investigated the inhibitory mechanism of the ß-lactamase inhibitor sulbactam, as well as the effect of the antibiotic ceftriaxone on BlaC with mix-and-inject *tr*-SFX. The substrate, sulbactam or ceftriaxone solution was mixed with the BlaC microcrystals at the mixing point ($\Delta t$ = 0) in the mixing injector. The reaction, initiated by ligand diffusion, was probed with X-rays at various delay times ($\Delta t_x = t_1, t_2, t_3, \ldots, t_n$), where $\Delta t_x$ is the time difference between the probing X-rays in the interaction region and the mixing starting point $\Delta t_0$. This


https://doi.org/10.1021/acscatal.4c02526
ACS Catal. 2024, 14, 10853−10870

approach enabled recording of reaction intermediates of BlaC with ceftriaxone with delay times ranging between 3 ms and 2 s.[41,104] For instance, Figure 3 shows the evolution of the

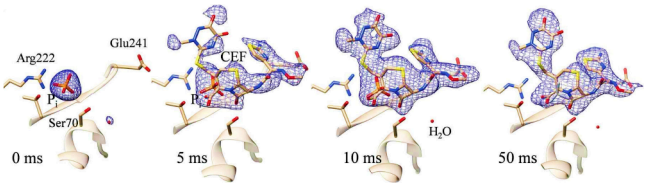


**Figure 3.** An example of an MISC experiment conducted at the SPB/SFX instrument of the European XFEL. The first MISC *tr*-SFX on ß-lactamase BlaC enzymatic catalysis to achieve a single millisecond temporal resolution,[41] in which a series of events of a ceftriaxone antibiotic substrate binding to the active Ser70 residue in subunit B are tracked and recorded with ultrashort XFEL pulses from 0 ms (the reference structure of the enzyme-free state) to 50 ms, where the CEF gradually substituted the inorganic phosphate in the active site to reach a dominant occupancy at ∼10 ms. The appearance of a partial CEF substrate was observed for 5 ms. The blue mesh represents the enhanced polder maps contoured at the 3.0 $\sigma$ level. This figure is adapted from ref 41. Copyright 2021 IUCTJ.

antibiotic ceftriaxone (CEF) with increasing delay time, starting from zero occupancy of the substrate (CEF) at $\Delta t$ = 0 (which represents a structure without substrate) to 100% occupancy in the catalytic center of BlaC ($\Delta t$ > 50 ms). At this point, the catalytic residue Ser70 of BlaC hydrolyzes ceftriaxone and cleaves the dioxotriazine head, thereby helping to elucidate the molecular mechanism of BlaC and the kinetics of CEF binding and release of modified CEF as a product.[41,104] By altering the delay time between the mixing region and the X-ray interaction point, e.g., by changing the distance to the X-ray interaction point, conformational changes in the active site upon substrate binding can be observed. This observation can be used to gain insight into the underlying biochemical processes involved. The information required to determine the conformation at a specific delay time ($\Delta t$) includes the fractional concentration (occupancy) at that specific delay time and the reference structure, which is the protein structure without substrate in the resting state. In other words, the required information is the isomorphous difference electron density (DED) map obtained from the refined structures of the isomorphous pair (reference structure factor amplitudes $|F_{free}^{Obs}|$ for the enzyme-free state and substrate-bound models $|F_{t}^{Obs}|$, which accounts for the relative accumulation of an intermediate at a specific delay time, $\Delta t$, after reaction initiation) (see refs 93, 106 for recent accounts on *tr*-SFX data processing and extraction of transiently formed intermediate states).

In redox enzyme catalysis, following redox triggering through substrate mixing, the enzyme undergoes subtle to large conformational rearrangements in the catalytic cleft of the redox center and, in some cases, over long-range distances. This enables the trapping of redox intermediate states, as demonstrated in the case of bovine cytochrome *c* oxidase (*Cc*O) microcrystals during reaction with molecular oxygen ($O_2$).[77] *Cc*O oxidoreductase is an essential metabolic redox enzyme responsible for catalyzing the four-electron reduction of $O_2$ into two water molecules through several intermediate states. The system uses the generated redox energy to pump four protons across the membrane through an electrochemical gradient (downhill), thereby generating a proton electrochemical potential, which is used by ATP synthase to synthesize ATP molecules.[78,107−109] Using a T-shaped mixing injector, a buffer saturated with $O_2$ was mixed with fully reduced *Cc*O microcrystals before probing the reaction intermediate with 40 fs X-ray pulses 8 s after the $O_2$ diffusion. This slower delay time was controlled by a mixer loop, and the time was chosen based on *in crystallo* optical spectroscopy data. However, given the microcrystal dimensions (20 × 20 × 4 $\mu m^3$) used in the experiment and the size and chemical nature of $O_2$, diffusion was estimated to occur within approximately 2 ms, several orders of magnitude faster than the accumulation of the reaction intermediate.[77] Such faster substrate diffusion is critical not only for scanning the primary intermediates of certain reactions but also for capturing the transitions between different intermediates, which are important for obtaining an overall understanding of biochemical reactions. Large conformational changes were observed upon redox reaction *in crystallo*, particularly in the local vicinity of heme *a*. These changes included flipping (swinging) of nearby residues and a change in the farnesyl side chain of heme *a* cofactor as well as large-scale motion and rotation of some key residues, implying that redox electron transfer event(s) may induce noticeable conformational changes in the catalytic site that are useful for inferring the catalytic mechanism.[77] Such information offers direct insight into redox enzyme catalysis when combined with individual redox state structures, i.e., fully reduced and oxidized states, as has been demonstrated for *Cc*O and the NADPH-cytochrome P450 reductase.[77,78,109,110] By using MISC *tr*-SFX, it was also possible to observe the gating conformational dynamics of the redox hydrolase enzyme isocyanide hydratase (ICH) during catalysis, resolving a set of correlated conformational changes, i.e., nonequilibrium protein motions, that alter the ICH active site and increase catalytic efficiency.[83] ICH catalyzes the irreversible reaction of isocyanide hydration to form N-formamide from a cysteine-derived thioimidate intermediate.[83,84] Microcrystals of ICH were mixed with a para-nitrophenyl isocyanide (*p*-NPIC) substrate using a coMESH microfluidic T-junction mixing injector to the X-ray interaction region after 15 s and 5 min delay times. Isomorphous difference maps of $|F_{15s}^{obs}-F_{free}^{obs}|$, calculated using the structure factor phases of the enzyme-free state ($\varphi_{free}$), showed widely distributed conformational changes across ICH upon cysteine (Cys101) modification, i.e., thioimidate intermediate formation between the sulfhydryl group of Cys101 and the *p*-NPIC substrate, indicating the importance of these changes in ICH catalysis.[83,84]

A drop-on-demand tape-drive-based sample delivery method was used to collect *tr*-SFX data on isopenicillin *N*-synthase (IPNS) with catalytic ferrous ions ($Fe^{2+}$), revealing the catalytic events of the reaction of L-$\delta$-($\alpha$-aminoadipoyl)-L-cysteinyl-D-valine (ACV) with dioxygen to form isopenicillin (IPN), the precursor for all penicillin and cephalosporin antibiotics.[82] ACV substrate-bound fully reduced (IPNS:Fe(II):ACV) anaerobic microcrystal slurries were exposed to atmospheric $O_2$, and redox intermediates were probed with X-rays at different delay times from 400 ms to 3.0 s via simultaneous collection of *tr*-SFX and *tr*-XES (time-resolved X-ray emission spectroscopy) data using a similar setup to that used for photosystem II.[56] The delay time was controlled by the speed of the Kapton tape. Enzyme dynamics involving long-range conformational changes essential for the conversion of ACV to IPN were observed. Intriguingly, $O_2$ binding was found to alter the crystal lattice and induce motion beyond


https://doi.org/10.1021/acscatal.4c02526
ACS Catal. 2024, 14, 10853−10870

those at the active site, causing dynamic changes throughout the IPNS.[82] A 50% increase in the temperature factor (*B*-factor) was observed at peripheral regions of the IPNS, which was consistent with the increase in $O_2$ binding. Importantly, the *B*-factor returned to its ground state upon the formation of the end product IPN and the removal of two water molecules, i.e., full consumption of the reactive dioxygen. Such comprehensive analysis is inevitable, especially when dissecting the catalysis of redox enzymes, as the dynamics associated with single or multiple electron transfers upon substrate binding play critical roles in tuning catalysis and may entail conformational changes throughout the protein.[111] Very recently, Nguyen et al. improved upon their drop-on-drop method for studying biochemical reactions *in crystallo* by including a second droplet dispenser. This approach enabled them to drop a tiny volume of droplets (in picoliter) of a second substrate, peracetic acid, containing hydrogen peroxide, on a large drop of microcrystalline slurry of *M. tuberculosis* cytochrome P450 (in nanoliter) with its native substrate (L-tyrosine-L-tyrosine, cYY) at different delay times, thereby enabling rapid mixing and subsequent reaction initiation before probing the triggered reaction with X-rays. As a result of such important developments in the MISC *tr*-SFX, an enzyme–substrate [*E*•*S*] complex of P450-based ferric-hydroperoxo (compound 0), a long-awaited high-spin intermediate that was not feasible before, was captured *in crystallo* at an ∼200 ms delay time, and the structure was resolved at a resolution of 1.85 Å (Figure 4). Shorter delay times were achieved by reducing the distance between the mixing point and the X-ray interaction region.[112]

## *IN CRYSTALLO* ENZYME KINETICS BASED ON MIX-AND-INJECT *TR*-SFX

Recent results on structural enzymology using the MISC *tr*-SFX technique provide a comprehensive and detailed understanding of the processing and interpretation of MISC data, thus enabling scientists to extract essential structural information on the different transient-kinetic states during the catalytic cycles of these enzymes.[41,104−106] MISC *tr*-SFX enables direct estimation of enzyme kinetics, as previously demonstrated in BlaC $\beta$-lactamase microcrystals, by directly observing the early events of enzyme and substrate complex [*E*·*S*] formation at a single millisecond temporal resolution. The fully saturated enzymatic active site shows the formation of CEF (aminothiazole and dioxotriazine) with the BlaC catalytic residue Ser70 after approximately 50 ms and partial formation of the reaction product, as indicated by the weakened electron density of the CEF density map.[41,97,104,105] By combining very short and longer delay times and probing intermediates with sufficiently short intervals, it becomes possible to delineate the complete enzymatic reaction steps, from the formation of the enzyme–substrate complex (*E*·*S*) to the decomposition of *E*·*S*, resulting in the regeneration of the free enzyme (*E*) and the release of the reaction product (*P*) (Figure 5). This enables a reasonable estimation of the reaction kinetics *in crystallo* by following the Michaelis–Menten (MM) approximation model. Here, the reaction rate ($\upsilon$) is defined as $\upsilon = \frac{V_{max}[S]}{K_m + [S]}$, where $V_{max}$ is the maximal velocity reached at high substrate concentrations for a given enzyme concentration [*E*] (i.e., when all active sites of the enzyme in the crystal are occupied by substrates reaching a 1:1 stoichiometric state, assuming a

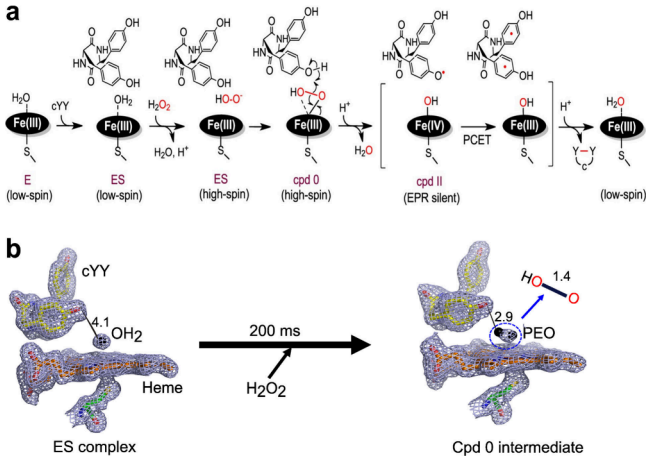


**Figure 4.** Reaction pathway of cytochrome P450 CYP121 and the *in crystallo tr*-SFX intermediate structures. a) Proposed pathway for the catalytic reaction of CYP121 on the native substrate cYY. b) Low-spin ES complex before the addition of an oxidant ($H_2O_2$) and trapping of the high-spin Cpd0 intermediate after 200 ms of mixing and delay time (drop-on-demand mixing of *tr*-SFX). The formation of the ferric hydroperoxo (PEO) of Cpd 0 facilitated hydrogen bond formation with the substrate cYY, suggesting its direct role in the C−C coupling cyclization of the substrate via a mechanism that is not common in heme enzymes.[112] The distances in panel b are in Å. Panel a is adapted from ref 112. Copyright 2023 American Chemical Society.

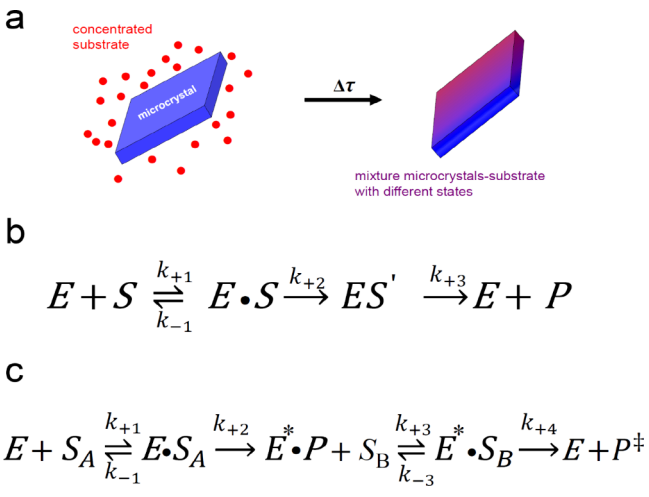


**Figure 5.** Diffusion of the substrate into microcrystals and two possible kinetic mechanisms *in crystallo* following single-substrate or two-substrate diffusion. a) A highly concentrated substrate on the immediate surface of a microcrystal diffuses quickly as the diffusion time increases in proportion to the crystal size in the flux direction from a high concentration (outside surface) to a low concentration (inside microcrystals), allowing quick binding of the substrate. b) Standard enzymatic mechanism with a single-substrate reaction showing the binding kinetics of the forward ($K_{+1}$) and reverse ($K_{-1}$) pathways and the formation of the enzyme–substrate complex intermediates [*E*·*S*] and [*ES*′], which accumulate in crystallo at different delay times after mixing, as well as the turnover constant ($K_{+3}$). c) Example of a two-substrate Ping-pong reaction-like mechanism displaying the formation of an enzyme–substrate A ($S_A$) complex, an intermediate product (an activated enzyme with the first product *P* [*E**·*P*]), an enzyme–substrate B complex and the formation of the second product ($P^{\ddagger}$).


https://doi.org/10.1021/acscatal.4c02526
ACS Catal. 2024, 14, 10853−10870

first-order reaction). The Michaelis constant $K_m$ is calculated as $K_m = \frac{(K_{-1} + K_{+3})}{K_{+1}}$, representing the substrate concentration at which the enzymatic rate equals half of $V_{max}$ (refer to Figure 5b).[63,104,105] Here, the forward ($K_{+1}$) and reverse ($K_{-1}$) rate constants and the catalytic rate constant ($K_{+3}$) (i.e., $K_{cat}$) are unknown and can be estimated based on the substrate diffusion time, concentration, and rate of product formation. It should be noted, however, that the majority of the enzymatic reactions have a moderate turnover rate of ~10 $s^{-1}$,[191] meaning that the currently achieved temporal resolution is suitable to cover the dynamics of most of these enzymes. However, for fast enzymatic turnover kinetics ($1/K_{cat}$), such as those of the metalloenzymes catalase (~$4 \times 10^7$ $s^{-1}$) and carbonic anhydrase ($10^4$ to $10^6$ $s^{-1}$), which are on the order of microseconds, the diffusion time is much slower than that for the formation of reaction intermediates. This makes it extremely challenging to capture their intermediates with the currently available technology.[87,100]

The mixing of the substrate with the enzyme *in crystallo* can be considered similar to the stopped flow method in solution, with the major difference being that the substrate diffuses much faster than *in crystallo*.[113−115] The diffusion of the substrate adopts Fick's second law (Laplace's equation): $D\nabla^2 C = \frac{\partial c}{\partial \tau}$, where the diffusion coefficient $D$ defines the amount of substrate $C$ that diffuses from the highest concentration region (surface of the crystals assuming homogeneous distribution before mixing) across a unit area (in this case, it is a 3D microcrystal with defined dimensions) in a unit of time, and $\nabla^2$ is the Laplacian, which is defined as $\nabla^2 = \frac{\partial^2}{\partial x^2} + \frac{\partial^2}{\partial y^2} + \frac{\partial^2}{\partial z^2}$ for a spatial flux of substrate in 3D box-like objects (e.g., protein microcrystals).[100,104] Substrates are used at sufficiently high concentrations (up to ~15 times higher than the enzyme concentrations in crystals) to ensure rapid diffusion (i.e., increasing the osmotic pressure).[100,112] Olmos et al. estimated that the stoichiometric ratio of BlaC:CEF can be reached at a time $t = t_D \cdot f$, where $t_D$ is the diffusion time and $f = -\ln\left(1 - \frac{[S]_{in}}{[S]_{out}}\right)$, in which $[S]$ is the substrate concentration inside and outside the crystal.[104] This means that a 1:1 stoichiometric ratio between the substrate and the enzyme *in crystallo* can occur at a much faster delay time than that of diffusion.

Notably, the biomolecules (e.g., enzymes) *in crystallo* are densely crowded and highly packed in a crystallographic unit cell, which can, in some cases, result in limited solvent access channels.[116,117] Such steric confinement occasionally prevents effective diffusion of relatively large enzyme substrates and ligands into crystals, resembling the macromolecular crowding state, which decreases the diffusion rate and affects enzyme−substrate interactions, with the exception that crowded crystalline proteins or enzymes are highly ordered and remain in close contact with weak interactions, i.e., spatially organized molecules.[118−120] Therefore, identifying crystallization conditions for target enzymes that preserve solvent accessibility channels and flexibility is crucial. This allows for effective diffusion while maintaining high-quality diffraction without causing changes or deformations in the crystalline order, which could complicate the processing and extraction of meaningful information from MISC *tr*-SFX data. It is also necessary to take the differences between *solution* and the *crystalline* environment into consideration when interpreting *tr*-SFX data, as reaction kinetics *in solution* are not necessarily similar to those *in crystallo*.

Notably, based on currently available mixing delivery systems,[42,82,83,112,121−123] the above-mentioned discussion holds true only for the MM kinetics of a standard single-substrate enzymatic reaction (Figure 5b). This approach is not applicable when considering enzymatic reactions involving two or more substrates, which is the case for many enzymes, such as those following the ping-pong bibi (double-displacement) or sequential mechanism.[124,125] One classical example of such enzymes is the heme peroxidase superfamily, which includes dye-decolorizing peroxidases (DyPs) and adopts a double-substrate ping-pong kinetic model.[126] The resting state of DyPs is initially oxidized by hydrogen peroxide (substrate 1 ($S_A$)) by abstracting one electron from heme-$Fe^{3+}$ to form a reactive transient intermediate with high-valent heme species (compound I) (i.e., ferryl heme or [$Fe^{4+}$=oxo] together with porphyrin $\pi$-cation radical species), an activation step essential for the subsequent oxidative catalysis of reducing substrate 2 ($S_B$) (i.e., synthetic dyes, lignin, and other chemical species such as carotenoids) and the formation of the second transient intermediate (compound II or $Fe^{4+}$=oxo) by abstracting an electron from substrate 2. The reduction of compound II by another substrate 2 regenerates the resting state.[55,127−131] In recent static room-temperature SFX studies, radiation damage-free structures were successfully obtained, and significant details on the redox structures of the different transient states were explored to determine the chemistry of various DyPs, dehaloperoxidase B, and cytochrome *c* peroxidase, among other metalloenzymes.[14,128,132] These studies adopted a soaking method of peroxidase microcrystals with peroxide or peroxybenzoic acid to prepare ferryl heme species from the target transient intermediate (i.e., compound II) and presented evidence that the compound II intermediate state differs among different peroxidases, highlighting differences in the hydrogen bonding network and the bond lengths of the $Fe^{4+}$=oxo species.[14] However, the dynamics and conformational changes that occur in the catalytic centers of these metalloenzymes during catalysis have not yet been revealed. This is largely due to the lack of a suitable triggering method for *tr*-SFX or the insufficiency and difficulties associated with currently available methods such as MISC *tr*-SFX or photocaging. It is also difficult to trap the transient state of compound I because it spontaneously decays to compound II on time scales in the absence of an exogenous electron donor, which is most often infeasible to probe at ambient temperatures and is enabled only by the cryotrapping method, which prevents further decay.[133,134] Here, we propose that developing a sophisticated mixing injector for complex mix-and-inject *tr*-SFX (*c*MISC) experiments could pave the way for unraveling the dynamics and kinetics of metalloenzymes that adopt double-substrate or multisubstrate mechanisms. The development of such a tool will enable the trapping of fast transient intermediates, which have proven to be elusive using conventional crystallographic methods.

Two scenarios appear to be feasible for the complex MISC (*c*MISC): (i) Presoaking the microcrystals with the first substrate ($S_A$) to generate the first enzymatic intermediate. Subsequently, a slurry of reaction-activated microcrystals was used to initiate the next reaction steps by mixing the mixture with the second substrate ($S_B$) before the enzymatic cycles were probed with X-rays, and (ii) the two substrates were


https://doi.org/10.1021/acscatal.4c02526
ACS Catal. 2024, 14, 10853−10870

mixed on the fly, while the delay times were tuned. This allows $S_A$ to diffuse first, thereby activating the enzyme *in crystallo* followed by a second mixing with $S_B$ in a defined delay time before the chemical reactions were probed with X-rays (Figure 5a). Alternatively, both substrates and enzymes can be mixed simultaneously using a single mixer to mix the substrates and enzymes immediately before jetting the mixture into the X-ray interaction region (Figure 5b). Currently, to the best of our knowledge, there is no such microfluidic device that satisfies the second proposal of cMISCs. Moreover, the first scenario is possible only for cases where the formed intermediate is stable; it is unfeasible, for instance, where the transiently formed intermediate is unstable and decays rapidly to other intermediates. One of the challenges that may be encountered with the *c*MISC method is the synchronization of the diffusion of $S_A$ and $S_B$ in the microcrystals. How to fine-tune the timing of the diffusion of both substrates and reduce the artifacts that may occur when the first model is applied (Figure 4a) will facilitate the downstream data processing of the different delay times. This approach will eventually provide a sensible biochemical interpretation of the data. In the second case, the limitation relies mostly on whether it is important for $S_A$ to bind first or not to allow proper enzymatic catalysis (Figure 5b). The *c*MISC technique can also be applied using a drop-on-demand tape-drive delivery system[82] to study slower enzymatic cycles. This can be achieved, for instance, by applying sequential or synchronized droppings of different substrates with a well-defined spacing on the same droplet of microcrystals before probing the initiated reaction with X-rays. Here, the synchronization of substrate droplets with microcrystals during a tape drive can be challenging. While preparing for the submission of this perspective, Nguyen et al. reported interesting results on P450 reductase, applying a similar approach to that of the first scenario.[112]

## CHALLENGES AND FUTURE FOCUS

We reviewed recent advances in *tr*-SFX using a diffusion-based method known as mix-and-inject *tr*-SFX and highlighted the current achievements in studying the structure and dynamics of nonphotoactive metalloenzymes. In addition, we discussed the opportunities and challenges in obtaining crystallographic kinetic information via this method. Mix-and-inject *tr*-SFX is the only available versatile method applicable to all light nonresponsive proteins and can directly trigger the biochemical reaction of target proteins *in crystallo* by mixing with its native substrate(s) and probing the formation of reaction intermediates at well-defined and controllable delay times upon substrate binding.[97,100] One of the major challenges in MISC *tr*-SFX, however, is the inevitable requirement for a large number of indexed images of highly isomorphous microcrystals to ensure high accuracy for the reflection intensities within and between the different delay times.[93,106,135−138] Achieving such a tedious goal may require initially growing homogeneous and highly isomorphous microcrystals and obviously several days of continuous diffraction data collection with reasonable stability in the XFEL sources given the limitation of beamtime availability in XFEL sources. The SACLA, SwissFEL, PAL-XFEL, and LCLS XFEL sources operate at repetition rates in the 10−120 Hz range, which limits the number of delay times (i.e., reaction intermediates) needed to be collected in a given beamtime, which is usually 2 days to full week of data collection.[139−143] The European XFEL is the only running facility that operates at high repetition rates up to 4.5 MHz.[144] With the SPB/SFX instrument, we operate maximally at 1.13 MHz for SFX experiments with up to 352 pulses per train (10 Hz) (see, for example, Figure 1),[38,144,146] enabling the recording of diffraction data at 1.2 million images per 5 min of run.[36−38,40,145] This unique capability of the SPB/SFX Instrument of the European XFEL opens opportunities for collecting *tr*-SFX data with full reaction cycles in an unprecedented short beamtime and has been the key to achieving successful *tr*-SFX experiments using MISC and laser excitation.[37,38,146]

It is also challenging to obtain sub-millisecond temporal resolutions for ultrafast enzymatic reactions such as bond breaking owing to the difficulties associated with the limitations of mixing devices as well as because crystals that are too small may not diffract given the current limitations in photon fluxes.[41,100,122] It is possible to compensate for such limitations with, for example, high substrate concentrations and crystal size optimization. Well-diffracting microcrystals with sizes less than $2 \times 2 \times 2\ \mu m^3$ in combination with ∼20 times higher concentrations of the substrate can achieve delay times of several hundred microseconds.[135] Smaller diffraction crystals down to the nanoscale will ensure uniform diffusion and a populated intermediate at the respective delay times, which is essential for successful MISC *tr*-SFX experiments and *in crystallo* kinetics analysis.[100] As some biochemical reactions can progress at rates down to several seconds, it is important to cover slower delay times to obtain a comprehensive understanding of the enzymatic cycles of some processes. While this approach is feasible for certain delivery systems that operate at low repetition rates, such as the on-demand, drop-on-drop method (from 0.6 to 2 s)[147] and those used for synchrotron-based time-resolved serial crystallography, such as the Spitrobot plunger for cryo-trapped intermediates (from 0.05 to 30 s) and the liquid application method for time-resolved analyses at synchrotron (LAMA setup) (0.015 to 60 s),[98,148] it is not practical for facilities operating at high repetition rates. Achieving this would likely require significant modification in the device to slow the arrival time of the mixed crystalline slurries or simply operate at low repetition rates. At the SPB/SFX instrument, two interaction regions exist: upstream and downstream. The latter is dedicated to experiments that operate at low repetition rates and for samples that require high-viscosity extruder devices (HVEs) to jet, such as membrane protein microcrystals embedded in the viscous lipid cubic phase.[36,149] We recently succeeded in developing a mixing-HVE device that can achieve mixing times of 2 to 20 s, and this was demonstrated via a fluorescence quenching experiment on iq-*m*Emerald fluorescent protein microcrystals.[123] It is possible to use mixing-HVE devices with various viscous materials, such as grease or Vaseline,[150−152] agarose,[153] hydroxyethyl cellulose,[154] and lards,[155] which can cover a wide range of different metalloenzymes and membrane proteins without compromising their diffraction quality. This approach can serve as a complementary mixing device for longer delay times within a single facility, allowing us to cover delay times from a few milliseconds to several seconds; however, it is still tedious to run experiments that require a wide range of delay times (e.g., from microseconds to milliseconds), for example, running both interaction regions of the SPB/SFX instrument within a single dedicated beamtime.

Data processing of SFX has been challenging and often requires experts to quickly process the data and provide preliminary feedback to allow planning for the remaining


https://doi.org/10.1021/acscatal.4c02526
ACS Catal. 2024, 14, 10853−10870

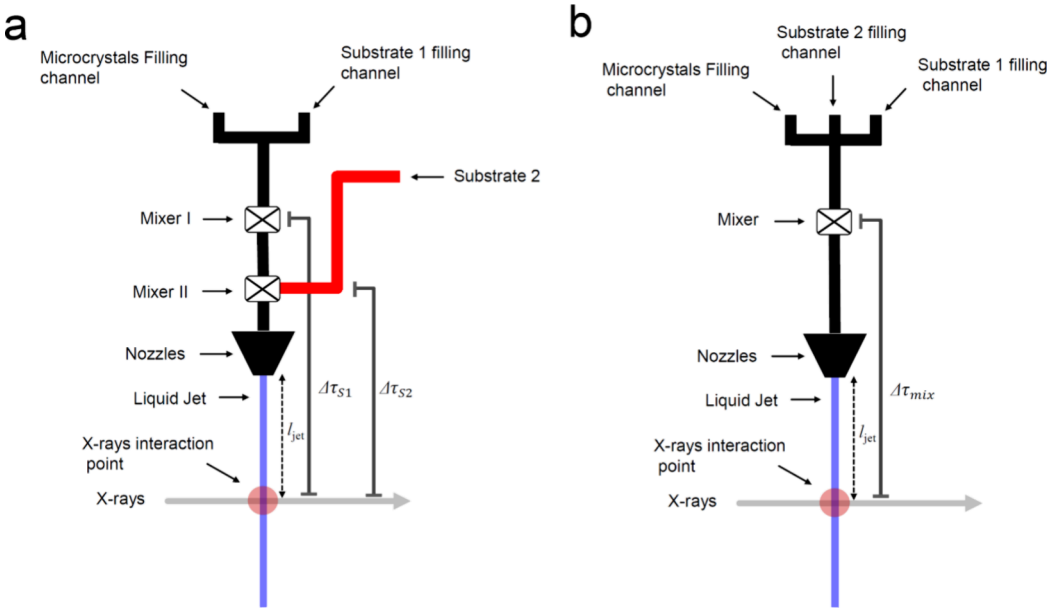


**Figure 6.** Schematic views of two proposed mixing injectors for complex mixing-and-inject (*c*MISC)*tr*-SFX. These cMISC injectors are suitable for studying enzyme catalysis with double substrates such as dye-decolorizing peroxidases. a) The design consists of two independent mixers for the two substrates with a defined spacing between mixers. Here, microcrystals and substrate 1 can be applied at the same time via separate channels to control their arrival at mixer I, which delays $\Delta t_{S1}$ to the X-ray interaction point; then, a third channel arrives at the same time for substrate 2 to mix with mixer II containing the mixed microcrystals. A delay time of $\Delta t_{S2}$ will define the diffusion time of substrate 2 with the activated enzyme. The delay times can then be controlled by the jet length ($l_{jet}$). b) This design consists of a single mixer with three independent channels for the microcrystals and substrates 1 and 2. The delay time here accounts for the diffusion of both substrates, which is controlled to arrive at the same time as for the microcrystals in the mixer.

experimental times, especially for *tr*-SFX data, to allow real-time selection of the appropriateness of the triggering strategy, e.g., when isomorphous signals are unobservable or when significant changes in the unit cell parameters have occurred due to mixing with a substrate. Several software programs are used to process SFX data: online data monitoring software such as *OnDa*;[156] offline data analysis tools such as *crystFEL*,[157,158] *Cheetah*,[159] *cctbx.xfel*,[160] *nXDS*,[161] *cppxfel*,[162] *psocake* at PAL-XFEL;[163] and the online/offline pipeline tool (adapted from crystFEL and Cheetah) at the SACLA.[164] At European XFEL, a semiautomated pipeline to streamline data processing has been developed recently based on *crystFEL*.[165,166] Nonetheless, dealing with *tr*-SFX data in general, including MISC data, has been extremely challenging. This is largely due to the difficulties associated with the analysis of small structure factor signals of the populated reaction intermediates, which often accumulate at specific times in fractions within the crystal unit cell, resulting in an ensemble of averaged accumulated structures of these fractions (~10 to 45% of reflection intensities and less than 20% in most cases).[66,167,168] More commonly, multiple intermediate states populate in a single microcrystal, especially at slower time scales; this phenomenon is also expected in cases where the intermediate state is unstable or decays simultaneously, such as when compound I decays into compound II in peroxidases,[133] resulting in several intermediate states in the averaged structure (i.e., structure factor intensities with mixed states) that are trapped at a single delay time.[105,169] In addition, the shot-to-shot heterogeneity, nonisomorphic unit cell parameters, and crystal orientation problems complicate further analysis of the *tr*-SFX data, leading to difficulties in detecting difference structure factor signals $\Delta|F|_t$.[106] Principal component analysis (PCA) methods such as single value decomposition (SVD) were used previously[170] to analyze time-resolved macromolecular X-ray data using photoactive yellow protein crystals and were successfully applied to pump−probe *tr*-SFX data.[37,168] SVD allows for unbiased differentiation between signals and noise, thereby enhancing the detection of small difference structure factor signals. Moreover, SVD is effective at deconvoluting various components of the enzymatic cycle and identifying different intermediates as well as decay or relaxation times based on differences in structure factor signals.[105,170] SVD can also provide information regarding the enzyme kinetics and thermodynamics of biochemical reactions.[171−173] Recently, Malla et al. used SVD to analyze MISC *tr*-SFX data collected from ß-lactamase-free products and from sulbactam inhibitors at several delay times between 3 and 700 ms.[105] Their SVD analysis, using the same set of MISC *tr*-SFX data, revealed not only the structural changes that occur within these temporal resolutions but also the ligand binding heterogeneity, induced fit, cooperativity, and conformational changes that facilitate the accommodation of the ligand in the binding pocket (an induced fit-like mechanism).[105,174] This opens opportunities to study the structural dynamics and enzymatic catalysis of many enzymes, including those of particular biomedical and pharmacological interest. In 2022, De Zitter et al. reported the *Xtrapol8* software tool, which uses a Bayesian-statistics weighting of the Fourier difference maps to improve the low occupancy signals of the structure factor amplitude differences between reference and triggered *tr*-SFX data.[175] This method can also differentiate between coexisting intermediate states in the same set of data, which is important in handling *tr*-SFX data. Although *Xtrapol8* has been applied only to pump−probe *tr*-SFX data, it may also be effective for MISC *tr*-SFX.


https://doi.org/10.1021/acscatal.4c02526
ACS Catal. 2024, 14, 10853−10870

It should be noted that even with a reliable data processing method, complementary computational methods such as first principle calculations are inevitable for a reliable interpretation of the biochemical function of the systems.[185] Understanding how enzymes catalyze the acceleration of chemical reactions and the conversion of substrates to diverse products is essential. It is also crucial to study these enzymes in different environments, such as under different crystalline conditions, in different solutions, and in crowded media. Such studies are fundamental to the general understanding of enzyme catalysis and a prerequisite for the efficient design of novel catalysts. To this end, integrating theoretical calculations and time-resolved experimental data can provide such a fundamental understanding.[185,187,188] The experimental conformational changes that evolve on different time scales in protein crystals are important for the molecular function of proteins; however, as such, changes may coexist in a specific time and space, especially in crystals, because the inherent inhomogeneity of reaction triggering can be extremely complex to retrieve and accurately interpret. Recently, a crystalline dynamic simulation was performed to generate calculated electron density maps by introducing crystal packing similar to that of photosystem II *tr*-SFX data, which not only reproduced the electron density dynamics of *tr*-SFX but also revealed structural changes beyond the experimental data. Adding to this is the application of the SVD method to MISC *tr*-SFX data on the BlaC enzyme, as described above, which enables the extraction of the temporal variation in the difference in electron density and hence can infer the multistate conformations, kinetics, and energetics of the reactions. Using numerical simulations, factors such as diffusion time in crystals of different sizes, time-dependent concentrations of intermediates, and magnitudes of reaction rate coefficients were simulated based on the crystalline environment and compared with experimental results.[100] With the currently available high computing power, using simulations can enhance the interpretation of the experimental *tr*-SFX data, unlock unique features in some cases, and provide new insights into the system under study. State-of-the-art methods such as Markov state models and *ab initio* molecular dynamics (AIMD) can be implemented to gain atomistic insights into the dynamics of biomolecules *in crystallo* or in solution. Accurate experimental data are also important for refining and enhancing the accuracy of computational methods.

## CONCLUSIONS

Here, we discuss recent works using the mix-and-inject *tr*-SFX method with a primary focus on prominent examples. We have also outlined the current challenges and ongoing efforts to cope with them. We envision that MISC *tr*-SFX, in combination with newly developed analysis and mixing injectors, will soon become a popular method of choice for studying the structural dynamics of proteins, particularly in the context of biocatalysis and the reaction kinetics of enzymes. This approach has the potential to significantly enhance our understanding of how enzymes function at the molecular level with high spatiotemporal resolution. Ongoing developments in the field of instrumentation, including our current proposals for *c*MISC *tr*-SFX, as well as the development of downstream data processing, will eventually broaden the applications of MISC *tr*-SFX and deepen our understanding of the structure and dynamics of biomolecules, notably biocatalysis.

The MISC *tr*-SFX method, despite having recently evolved following the advent of XFELs and still undergoing continuous development, has led to significant advances in the field of structural enzymology and contributed to the discovery of previously unknown structural mechanisms. This includes structural changes that unravel the mechanism of induced-fit, enzymatic heterogeneity, and the discovery of a reaction intermediate that was not known before, such as the trapping of compound 0 ($Fe^{3+}$-OOH), a long-sought reaction intermediate, in the crystalline state of cytochrome P450 reductase CYP121 with a native substrate. This high-spin ($S$ = 5/2) compound 0 intermediate has been challenging due to its high reactivity and short lifetime ranging from a few to less than a millisecond. This observation was only made possible using chemically modified substrates, i.e., halogenated substrate analogs, as demonstrated in the case of heme-dependent L-tyrosine hydroxylase and lactoperoxidase, where the halogen stabilizes the complex, thereby enabling its cryotrapping. Unexpectedly, in structurally trapped compound 0 of CYP121 with the native substrate cYY, unlike other heme-containing enzymes, the hydroperoxyl group was found in close proximity (~2.9 Å) to the substrate, suggesting the direct involvement of this intermediate in the oxidation and the C−C coupling cyclization of the substrate (Figure 4). This new finding in heme-based enzymology was enabled by the recent development of the on-demand rapid mixing injector method, which can achieve a temporal resolution of milliseconds. Moreover, using MISC *tr*-SFX with high temporal resolution, Schmidt and colleagues were able to structurally observe, for the first time, the ligand-gating, induced-fit structural ensembles, and conformational selectivity of an enzyme that was previously unattainable. This was made possible by the introduction of SVD to deconvolute the structural features of the enzyme-ligand complex *in crystallo* at different delay times. The authors demonstrate how the ligand enters the occluded binding pockets of two monomers selectively following a displacement of guarding residues, a mechanism that has not been described before, suggesting possibly a novel mechanism of ligand gating. These findings clearly demonstrate the potential of MISC *tr*-SFX for the study of structural enzymology. Multidimensional growth in the field of structural enzymology is foreseen in the near future with more MISC *tr*-SFX studies on different enzymes.

With MISC *tr*-SFX, it becomes feasible to probe the entire enzymatic cycle within the temporal range of single milliseconds to seconds of enzymatic catalysis, opening up opportunities for many nonphotoactive enzymes. To lead the field of time-resolved structural enzymology, however, MISC *tr*-SFX has to overcome the aforementioned challenges regarding rapid mixing, timing synchronization, and data analysis tools that enable the extraction of reliable reaction kinetics. It should also be emphasized here that the development of theoretical methods to model and simulate such complex structural data would complement and benefit the development of methods for broader use in the future. Overall, the structural visualization of enzyme catalysis will advance our basic understanding and pave the way toward efficient biomimetic catalysts or developing strategies to find effective medicines against an increasing number of multidrug-resistant enzymes. We finally hope that researchers interested in studying nonphotoactive enzymatic catalysis are well informed about the MISC *tr*-SFX technique and thus can employ it to explore fundamental questions in biocatalysis.


https://doi.org/10.1021/acscatal.4c02526
*ACS Catal.* 2024, 14, 10853−10870

## AUTHOR INFORMATION


### Corresponding Author

**Faisal H. M. Koua** − *European XFEL GmbH, D-22869 Schenefeld, Schleswig-Holstein, Germany*; Email: faisal.koua@xfel.eu

### Authors

**Huijong Han** − *European XFEL GmbH, D-22869 Schenefeld, Schleswig-Holstein, Germany*

**Richard Bean** − *European XFEL GmbH, D-22869 Schenefeld, Schleswig-Holstein, Germany*

Complete contact information is available at: https://pubs.acs.org/10.1021/acscatal.4c02526


### Author Contributions

FK conceptualized the perspective, reviewed the literature, and wrote the manuscript; FK and HH contributed to the editing of the manuscript; all authors reviewed and approved the final version of the manuscript.

### Notes

The authors declare no competing financial interest.

## ACKNOWLEDGMENTS

We thank all staff members of the SPB/SFX Instrument and the Sample Environment and Characterization Group of the European XFEL GmbH for helpful discussions during the preparation of this work. We would also like to acknowledge the European XFEL for the continuous support of our research programs.

## REFERENCES


(1) Neutze, R.; Wouts, R.; van der Spoel, D.; Weckert, E.; Hajdu, J. Potential for biomolecular imaging with femtosecond X-ray pulses. *Nature* **2000**, *406*, 752−757.

(2) Chapman, H. N.; Barty, A.; Bogan, M. J.; Boutet, S.; Frank, M.; Hau-Riege, S. P.; Marchesini, S.; Woods, B. W.; Bajt, S.; Benner, H.; et al. Femtosecond diffractive imaging with a soft-X-ray free-electron laser. *Nat. Phys.* **2006**, *2*, 839−843.

(3) Chapman, H. N.; Fromme, P.; Barty, A.; White, T. A.; Kirian, R. A.; Aquila, A.; Hunter, M. S.; Schulz, J.; DePonte, D. P.; Weierstall, U.; et al. Femtosecond X-ray protein nanocrystallography. *Nature* **2011**, *470*, 73−77.

(4) Chapman, H. N. X-ray Free-Electron Lasers for the Structure and Dynamics of Macromolecules. *Annu. Rev. Biochem.* **2019**, *88*, 35−58.

(5) Schlichting, I. Serial femtosecond crystallography: the first five years. *IUCrJ.* **2015**, *2*, 246−255.

(6) Chapman, H. N.; Caleman, C.; Timneanu, N. Diffraction before destruction. *Philos. Trans. R. Soc. London B Biol. Sci.* **2014**, *369* (1647), 20130313.

(7) Umena, Y.; Kawakami, K.; Shen, J.-R.; Kamiya, N. Crystal structure of oxygen-evolving photosystem II at a resolution of 1.9 Å. *Nature* **2011**, *473* (7345), 55−60.

(8) Koua, F. H.; Umena, Y.; Kawakami, K.; Shen, J. R. Structure of Sr-substituted photosystem II at 2.1 A resolution and its implications in the mechanism of water oxidation. *Proc. Natl. Acad. Sci. U.S.A.* **2013**, *110* (10), 3889−3894.

(9) Hirata, K.; Shinzawa-Itoh, K.; Yano, N.; Takemura, S.; Kato, K.; Hatanaka, M.; Muramoto, K.; Kawahara, T.; Tsukihara, T.; Yamashita, E.; et al. Determination of damage-free crystal structure of an X-ray-sensitive protein using an XFEL. *Nat. Methods* **2014**, *11* (7), 734−6.

(10) Lubitz, W.; Ogata, H.; Rüdiger, O.; Reijerse, E. Hydrogenases. *Chem. Rev.* **2014**, *114* (8), 4081−4148.

(11) Suga, S.; Akita, F.; Hirata, K.; Ueno, G.; Murakami, H.; Nakajima, Y.; Shimizu, T.; Yamashita, K.; Yamamoto, M.; Ago, H.; et al. Native structure of photosystem II at 1.95 Å resolution viewed by femtosecond X-ray pulses. *Nature* **2015**, *517*, 99−103.

(12) Nass, K.; Foucar, L.; Barends, T. R.; Hartmann, E.; Botha, S.; Shoeman, R. L.; Doak, R. B.; Alonso-Mori, R.; Aquila, A.; Bajt, S.; et al. Indications of radiation damage in ferredoxin microcrystals using high-intensity X-FEL beams. *J. Synchrotron. Radiat.* **2015**, *22* (2), 225−38.

(13) Ueno, G.; Shimada, A.; Yamashita, E.; Hasegawa, K.; Kumasaka, T.; Shinzawa-Itoh, K.; Yoshikawa, S.; Tsukihara, T.; Yamamoto, M. Low-dose X-ray structure analysis of cytochrome c oxidase utilizing high-energy X-rays. *J. Synchrotron Radiat.* **2019**, *26* (4), 912−921.

(14) Kwon, H.; Basran, J.; Pathak, C.; Hussain, M.; Freeman, S. L.; Fielding, A. J.; Bailey, A. J.; Stefanou, N.; Sparkes, H. A.; Tosha, T.; et al. XFEL crystal structures of peroxidase compound II. *Angew. Chem., Int. Ed. Engl.* **2021**, *60*, 14578−85.

(15) Yano, J.; Kern, J.; Sauer, K.; Latimer, M. J.; Pushkar, Y.; Biesiadka, J.; Loll, B.; Saenger, W.; Messinger, J.; Zouni, A.; et al. Where water is oxidized to dioxygen: structure of the photosynthetic Mn4Ca cluster. *Science* **2006**, *314* (5800), 821−5.

(16) Owen, R. L.; Rudino-Pinera, E.; Garman, E. F. Experimental determination of the radiation dose limit for cryocooled protein crystals. *Proc. Natl. Acad. Sci. U.S.A.* **2006**, *103*, 4912−4917.

(17) Garman, E. F. Radiation damage in macromolecular crystallography: What is it and why should we care? *Acta Crystallogr. D Struct. Biol.* **2010**, *66*, 339−351.

(18) Kern, J.; Yachandra, V. K.; Yano, J. Metalloprotein structures at ambient conditions and in real-time: biological crystallography and spectroscopy using X-ray free electron lasers. *Curr. Opin. Struct. Biol.* **2015**, *34*, 87−98.

(19) Garman, E. F.; Weik, M. Radiation Damage in Macromolecular Crystallography. *Methods Mol. Biol.* **2017**, *1607*, 467−489.

(20) Nass, K. Radiation damage in protein crystallography at X-ray free-electron lasers. *Acta Crystallogr. Sec. D* **2019**, *75*, 211−218.

(21) Suga, M.; Shimada, A.; Akita, F.; Shen, J.-R.; Tosha, T.; Sugimoto, H. Time-resolved studies of metalloproteins using X-ray free electron laser radiation at SACLA. *Biochim. Biophys. Acta Gen. Subj.* **2020**, *1864*, 129466.

(22) Hough, M. A.; Owen, R. L. Serial synchrotron and XFEL crystallography for studies of metalloprotein catalysis. *Curr. Opin. Struct. Biol.* **2021**, *71*, 232−238.

(23) Amin, M. Predicting the oxidation states of Mn ions in the oxygen-evolving complex of photosystem II using supervised and unsupervised machine learning. *Photosynth. Res.* **2023**, *156* (1), 89−100.

(24) Tanaka, A.; Fukushima, Y.; Kamiya, N. Two different structures of the oxygen-evolving complex in the same polypeptide frameworks of photosystem II. *J. Am. Chem. Soc.* **2017**, *139* (5), 1718−1721.

(25) Taberman, H. Radiation Damage in Macromolecular Crystallography—An Experimentalist's View. *Crystals* **2018**, *8*, 157.

(26) Lomb, L.; Barends, T. R.; Kassemeyer, S.; Aquila, A.; Epp, S. W.; Erk, B.; Foucar, L.; Hartmann, R.; Rudek, B.; Rolles, D.; et al. Radiation damage in protein serial femtosecond crystallography using an X-ray free-electron laser. *Phys. Rev. B Condens. Matter Mater. Phys.* **2011**, *84* (21), 214111.

(27) Gopakumar, G.; Unger, I.; Slavíček, P.; Hergenhahn, U.; Öhrwall, G.; Malerz, S.; Céolin, D.; Trinter, F.; Winter, B.; Wilkinson, I.; et al. Radiation damage by extensive local water ionization from two-step electron-transfer-mediated decay of solvated ions. *Nat. Chem.* **2023**, *15* (10), 1408−1414.

(28) Garman, E. F.; Weik, M. Radiation damage to biological macromolecules. *Curr. Opin. Struct. Biol.* **2023**, *82*, 102662.

(29) Bowman, S. E.; Bridwell-Rabb, J.; Drennan, C. L. Metalloprotein Crystallography: More than a Structure. *Acc. Chem. Res.* **2016**, *49* (4), 695−702.

(30) Liu, J.; Chakraborty, S.; Hosseinzadeh, P.; Yu, Y.; Tian, S.; Petrik, I.; Bhagi, A.; Lu, Y. Metalloproteins containing cytochrome,

iron-sulfur, or copper redox centers. *Chem. Rev.* **2014**, *114* (8), 4366−469.
(31) Orville, A. M. Recent results in time resolved serial femtosecond crystallography at XFELs. *Curr. Opin. Struct. Biol.* **2020**, *65*, 193−208.
(32) Barends, T. R. M.; Stauch, B.; Cherezov, V.; Schlichting, I. Serial femtosecond crystallography. *Nat. Rev. Methods Primers* **2022**, *2*, 59.
(33) Bergmann, U.; Kern, J.; Schoenlein, R. W.; Wernet, P.; Yachandra, V. K.; Yano, J. Using X-ray free-electron lasers for spectroscopy of molecular catalysts and metalloenzymes. *Nat. Rev. Phys.* **2021**, *3*, 264−282.
(34) Fukuda, Y.; Tse, K. M.; Suzuki, M.; Diederichs, K.; Hirata, K.; Nakane, T.; Sugahara, M.; Nango, E.; Tono, K.; Joti, Y.; et al. Redox-coupled structural changes in nitrite reductase revealed by serial femtosecond and microfocus crystallography. *J. Biochem.* **2016**, *159* (5), 527−538.
(35) Fukuda, Y.; Tse, K. M.; Nakane, T.; Nakatsu, T.; Suzuki, M.; Sugahara, M.; Inoue, S.; Masuda, T.; Yumoto, F.; Matsugaki, N.; et al. Redox-coupled proton transfer mechanism in nitrite reductase revealed by femtosecond crystallography. *Proc. Natl. Acad. Sci. U.S.A.* **2016**, *113* (11), 2928−2933.
(36) Mancuso, A. P.; Aquila, A.; Batchelor, L.; Bean, R. J.; Bielecki, J.; Borchers, G.; Doerner, K.; Giewekemeyer, K.; Graceffa, R.; Kelsey, O. D.; et al. The Single Particles, Clusters and Biomolecules and Serial Femtosecond Crystallography instrument of the European XFEL: Initial installation. *J. Synchrotron Radiat.* **2019**, *26*, 660−676.
(37) Pandey, S.; Bean, R.; Sato, T.; Poudyal, I.; Bielecki, J.; Cruz Villarreal, J.; Yefanov, O.; Mariani, V.; White, T. A.; Kupitz, C.; et al. Time-resolved serial femtosecond crystallography at the European XFEL. *Nat. Methods* **2020**, *17* (1), 73−78.
(38) Wiedorn, M. O.; Oberthür, D.; Bean, R.; Schubert, R.; Werner, N.; Abbey, B.; Aepfelbacher, M.; Adriano, L.; Allahgholi, A.; Al-Qudami, N.; et al. Megahertz serial crystallography. *Nat. Commun.* **2018**, *9* (1), 4025.
(39) de Wijn, R.; Melo, D. V. M.; Koua, F. H. M.; Mancuso, A. P. Potential of Time-Resolved Serial Femtosecond Crystallography Using High Repetition Rate XFEL Sources. *Appl. Sci.* **2022**, *12*, 2551.
(40) Mills, G.; Bean, R.; Mancuso, A. P. First Experiments in Structural Biology at the European X-ray Free-Electron Laser. *Appl. Sci.* **2020**, *10*, 3642.
(41) Pandey, S.; Calvey, G.; Katz, A. M.; Malla, T. N.; Koua, F. H. M.; Martin-Garcia, J. M.; Poudyal, I.; Yang, J. H.; Vakili, M.; Yefanov, O.; et al. Observation of substrate diffusion and ligand binding in enzyme crystals using high-repetition-rate mix-and-inject serial crystallography. *IUCrJ.* **2021**, *8* (6), 878−895.
(42) Vakili, M.; Bielecki, J.; Knoška, J.; Otte, F.; Han, H.; Kloos, M.; Schubert, R.; Delmas, E.; Mills, G.; de Wijn, R.; et al. 3D printed device and infrastructure for liquid sample delivery at the European XFEL. *J. Synch. Rad.* **2022**, *29*, 331−346.
(43) Waldron, K. J.; Rutherford, J. C.; Ford, D.; Robinson, N. J. Metalloproteins and metal sensing. *Nature* **2009**, *460* (7257), 823−830.
(44) Haas, K. L.; Franz, K. J. Application of metal coordination chemistry to explore and manipulate cell biology. *Chem. Rev.* **2009**, *109* (10), 4921−60.
(45) Shelley, K. L.; Garman, E. F. Quantifying and comparing radiation damage in the Protein Data Bank. *Nat. Commun.* **2022**, *13* (1), 1314.
(46) Kojima, S.; Homma, M.; Kandori, H. Purification of the $Na^+$-Driven PomAB Stator Complex and Its Analysis Using ATR-FTIR Spectroscopy. *Methods Mol. Biol.* **2023**, *2646*, 95−107.
(47) Inoue, K.; Ono, H.; Abe-Yoshizumi, R.; Yoshizawa, S.; Ito, H.; Kogure, K.; Kandori, H. A light-driven sodium ion pump in marine bacteria. *Nat. Commun.* **2013**, *4*, 1678.
(48) Inoue, K.; Koua, F. H.; Kato, Y.; Abe-Yoshizumi, R.; Kandori, H. Spectroscopic study of a light-driven chloride ion pump from marine bacteria. *J. Phys. Chem. B* **2014**, *118* (38), 11190−11199.
(49) Zouni, A.; Witt, H. T.; Kern, J.; Fromme, P.; Krauss, N.; Saenger, W.; Orth, P. Crystal structure of photosystem II from *Synechococcus elongatus* at 3.8 A resolution. *Nature* **2001**, *409* (6821), 739−743.
(50) Milikisiyants, S.; Chatterjee, R.; Coates, C. S.; Koua, F. H. M.; Shen, J.-R.; Lakshmi, K. V. The structure and activation of substrate water molecules in the $S_2$ state of photosystem II studied by hyperfine sublevel correlation spectroscopy. *Energy Environ. Sci.* **2012**, *5*, 7747−7756.
(51) Chatterjee, R.; Milikisiyants, S.; Coates, C. S.; Koua, F. H.; Shen, J. R.; Lakshmi, K. V. The structure and activation of substrate water molecules in Sr(2+)-substituted photosystem II. *Phys. Chem. Chem. Phys.* **2014**, *16* (38), 20834−20843.
(52) Asada, M.; Nagashima, H.; Koua, F. H.; Shen, J. R.; Kawamori, A.; Mino, H. Electronic structure of S(2) state of the oxygen-evolving complex of photosystem II studied by PELDOR. *Biochim. Biophys. Acta* **2013**, *1827* (3), 438−445.
(53) Kato, Y.; Noguchi, T. Redox properties and regulatory mechanism of the iron-quinone electron acceptor in photosystem II as revealed by FTIR spectroelectrochemistry. *Photosynth. Res.* **2022**, *152* (2), 135−151.
(54) Han, G.; Huang, Y.; Koua, F. H.; Shen, J. R.; Westlund, P. O.; Messinger, J. Hydration of the oxygen-evolving complex of photosystem II probed in the dark-stable S1 state using proton NMR dispersion profiles. *Phys. Chem. Chem. Phys.* **2014**, *16* (24), 11924−11935.
(55) Kalkan, Ö.; Kantamneni, S.; Brings, L.; Han, H.; Bean, R.; Mancuso, A. P.; Koua, F. H. M. Heterologous expression, purification and structural features of native *Dictyostelium discoideum* dye-decolorizing peroxidase bound to a natively incorporated heme. *Front. Chem.* **2023**, *11*, 1220543.
(56) Kern, J.; Alonso-Mori, R.; Tran, R.; Hattne, J.; Gildea, R. J.; Echols, N.; Glöckner, C.; Hellmich, J.; Laksmono, H.; Sierra, R. G.; et al. Simultaneous femtosecond X-ray spectroscopy and diffraction of photosystem II at room temperature. *Science* **2013**, *340* (6131), 491−495.
(57) Koua, F. H. M.; Kandori, H. Light-induced structural changes during early photointermediates of the eubacterial Cl- pump Fulvimarina rhodopsin observed by FTIR difference spectroscopy. *RSC Adv.* **2016**, *6*, 383−392.
(58) Ono, T. A.; Noguchi, T.; Inoue, Y.; Kusunoki, M.; Matsushita, T.; Oyanagi, H. X-ray Detection of the Period-Four Cycling of the Manganese Cluster in Photosynthetic Water Oxidizing Enzyme. *Science* **1992**, *258* (5086), 1335−1337.
(59) Kato, N.; Mizuno, S.; Shiozawa, M.; Nojiri, N.; Kawai, Y.; Fukumoto, K.; Morikawa, T.; Takeda, Y. A large-sized cell for solar-driven $CO_2$ conversion with solar-to-formate conversion efficiency of 7.2%. *Joule* **2021**, *5*, 687−705.
(60) Saito, K.; Rutherford, A. W.; Ishikita, H. Energetics of proton release on the first oxidation step in the water-oxidizing enzyme. *Nat. Commun.* **2015**, *6*, 8488.
(61) Bogacz, I.; Makita, H.; Simon, P. S.; Zhang, M.; Doyle, M. D.; Chatterjee, R.; Fransson, T.; Weninger, C.; Fuller, F.; Gee, L.; et al. Room temperature X-ray absorption spectroscopy of metalloenzymes with drop-on-demand sample delivery at XFELs. *Pure Appl. Chem.* **2023**, *95* (8), 891−7.
(62) Sharma, V.; Jambrina, P. G.; Kaukonen, M.; Rosta, E.; Rich, P. R. Insights into functions of the H channel of cytochrome c oxidase from atomistic molecular dynamics simulations. *Proc. Natl. Acad. Sci. U.S.A.* **2017**, *114* (48), No. E10339-E10348.
(63) Kupitz, C.; Basu, S.; Grotjohann, I.; Fromme, R.; Zatsepin, N. A.; Rendek, K. N.; Hunter, M. S.; Shoeman, R. L.; White, T. A.; Wang, D.; et al. Serial time-resolved crystallography of photosystem II using a femtosecond X-ray laser. *Nature* **2014**, *513* (7517), 261−265.
(64) Tosha, T.; Nomura, T.; Nishida, T.; Saeki, N.; Okubayashi, K.; Yamagiwa, R.; Sugahara, M.; Nakane, T.; Yamashita, K.; et al. Capturing an initial intermediate during the P450nor enzymatic reaction using time-resolved XFEL crystallography and caged-substrate. *Nat. Commun.* **2017**, *8*, 1585.


https://doi.org/10.1021/acscatal.4c02526
*ACS Catal.* 2024, 14, 10853−10870

(65) Suga, M.; Akita, F.; Yamashita, K.; Nakajima, Y.; Ueno, G.; Li, H.; Yamane, T.; Hirata, K.; Umena, Y.; Yonekura, S.; Yu, L.-J.; et al. An oxyl/oxo mechanism for oxygen-oxygen coupling in PSII revealed by an X-ray free-electron laser. *Science* **2019**, *366*, 334−338.
(66) Suga, M.; Akita, F.; Sugahara, M.; Kubo, M.; Nakajima, Y.; Nakane, T.; Yamashita, K.; Umena, Y.; Nakabayashi, M.; Yamane, T.; et al. Light-induced structural changes and the site of O = O bond formation in PSII caught by XFEL. *Nature* **2017**, *543*, 131−135.
(67) Kern, J.; Chatterjee, R.; Young, I. D.; Fuller, F. D.; Lassalle, L.; Ibrahim, M.; Gul, S.; Fransson, T.; Brewster, A. S.; Alonso-Mori, R.; et al. Structures of the intermediates of Kok's photosynthetic water oxidation clock. *Nature* **2018**, *563* (7731), 421−425.
(68) Ibrahim, M.; Fransson, T.; Chatterjee, R.; Cheah, M. H.; Hussein, R.; Lassalle, L.; Sutherlin, K. D.; Young, I. D.; Fuller, F. D.; Gul, S.; et al. Untangling the sequence of events during the S2 → S3 transition in photosystem II and implications for the water oxidation mechanism. *Proc. Natl. Acad. Sci. U.S.A.* **2020**, *117*, 12624−12635.
(69) Dods, R.; Båth, P.; Morozov, D.; Gagnér, V. A.; Arnlund, D.; Luk, H. L.; Kübel, J.; Maj, M.; Vallejos, A.; Wickstrand, C.; et al. Ultrafast structural changes within a photosynthetic reaction center. *Nature* **2021**, *589* (7841), 310−314.
(70) Schröder, G. C.; Meilleur, F. Metalloprotein catalysis: structural and mechanistic insights into oxidoreductases from neutron protein crystallography. *Acta Crystallogr. D Struct. Biol.* **2021**, *77* (10), 1251−1269.
(71) Koua, F. H. M. Structural Changes in the Acceptor Site of Photosystem II upon $Ca^{2+}/Sr^{2+}$ Exchange in the $Mn_4CaO_5$ Cluster Site and the Possible Long-Range Interactions. *Biomolecules* **2019**, *9* (8), 371.
(72) Oteiza, P. I. Zinc and the modulation of redox homeostasis. *Free Radic. Biol. Med.* **2012**, *53* (9), 1748−1759.
(73) Hosseinzadeh, P.; Lu, Y. Design and fine-tuning redox potentials of metalloproteins involved in electron transfer in bioenergetics. *Biochim. Biophys. Acta* **2016**, *1857* (5), 557−581.
(74) Valasatava, Y.; Rosato, A.; Furnham, N.; Thornton, J. M.; Andreini, C. To what extent do structural changes in catalytic metal sites affect enzyme function? *J. Inorg. Biochem.* **2018**, *179*, 40−53.
(75) Katiyar, N. K.; Goel, G.; Hawi, S.; Goel, S. Nature-inspired materials: Emerging trends and prospects. *NPG Asia Mater.* **2021**, *13*, 56.
(76) Bhowmick, A.; Hussein, R.; Bogacz, I.; Simon, P. S.; Ibrahim, M.; Chatterjee, R.; Doyle, M. D.; Cheah, M. H.; Fransson, T.; Chernev, P.; et al. Structural evidence for intermediates during O2 formation in photosystem II. *Nature* **2023**, *617* (7961), 629−636.
(77) Ishigami, I.; Lewis-Ballester, A.; Echelmeier, A.; Brehm, G.; Zatsepin, N. A.; Grant, T. D.; Coe, J. D.; Lisova, S.; Nelson, G.; Zhang, S.; et al. Snapshot of an oxygen intermediate in the catalytic reaction of cytochrome *c* oxidase. *Proc. Natl. Acad. Sci. U.S.A.* **2019**, *116*, 3572−77.
(78) Ishigami, I.; Carbajo, S.; Zatsepin, N.; Hikita, M.; Conrad, C. E.; Nelson, G.; Coe, J.; Basu, S.; Grant, T.; Seaberg, M. H.; et al. Detection of a Geminate Photoproduct of Bovine Cytochrome c Oxidase by Time-Resolved Serial Femtosecond Crystallography. *J. Am. Chem. Soc.* **2023**, *145* (41), 22305−22309.
(79) Maestre-Reyna, M.; Yang, C. H.; Nango, E.; Huang, W. C.; Ngurah Putu, E. P. G.; Wu, W. J.; Wang, P. H.; Franz-Badur, S.; Saft, M.; Emmerich, H. J.; et al. Serial crystallography captures dynamic control of sequential electron and proton transfer events in a flavoenzyme. *Nat. Chem.* **2022**, *14* (6), 677−685.
(80) Barends, T. R.; Foucar, L.; Ardevol, A.; Nass, K.; Aquila, A.; Botha, S.; Doak, R. B.; Falahati, K.; Hartmann, E.; Hilpert, M.; et al. Direct observation of ultrafast collective motions in CO myoglobin upon ligand dissociation. *Science* **2015**, *350* (6259), 445−450.
(81) Barends, T. R.; Bhattacharyya, S.; Gorel, A.; Schiro, G.; Bacellar, C.; Cirelli, C.; Colletier, J.-P.; Foucar, L.; Grünbein, M. L.; Hartmann, E.; et al. Influence of pump laser fluence on ultrafast structural changes in myoglobin. *bioRxiv* **2022**, 2022.11.22.517513.
(82) Rabe, P.; Kamps, J. J. A. G.; Sutherlin, K. D.; Linyard, J. D. S.; Aller, P.; Pham, C. C.; Makita, H.; Clifton, I.; McDonough, M. A.; Leissing, T. M.; et al. X-ray free-electron laser studies reveal correlated motion during isopenicillin N synthase catalysis. *Sci. Adv.* **2021**, *7* (34), No. eabh0250.
(83) Dasgupta, M.; Budday, D.; de Oliveira, S. H. P.; Madzelan, P.; Marchany-Rivera, D.; Seravalli, J.; Hayes, B.; Sierra, R. G.; Boutet, S.; Hunter, M. S.; et al. Mix-and-inject XFEL crystallography reveals gated conformational dynamics during enzyme catalysis. *Proc. Natl. Acad. Sci. U.S.A.* **2019**, *116* (51), 25634−25640.
(84) Smith, N.; Dasgupta, M.; Wych, D. C.; Dolamore, C.; Sierra, R. G.; Lisova, S.; Marchany-Rivera, D.; Cohen, A. E.; Boutet, S.; Hunter, M. S.; et al. Changes in an Enzyme Ensemble During Catalysis Observed by High Resolution XFEL Crystallography. *Sci. Adv.* **2024**, *10* (13), No. eadk7201.
(85) Moffat, K. Time-resolved macromolecular crystallography. *Annu. Rev. Biophys. Biophys. Chem.* **1989**, *18*, 309−32.
(86) Neutze, R.; Moffat, K. Time-resolved structural studies at synchrotrons and X-ray free electron lasers: opportunities and challenges. *Curr. Opin. Struct. Biol.* **2012**, *22* (5), 651−9.
(87) Schmidt, M. Time-Resolved Macromolecular Crystallography at Pulsed X-ray Sources. *Int. J. Mol. Sci.* **2019**, *20*, 1401.
(88) Pandey, S.; Poudyal, I.; Malla, T. N. Pump-Probe Time-Resolved Serial Femtosecond Crystallography at X-ray Free Electron Lasers. *Crystals* **2020**, *10*, 628.
(89) Aller, P.; Orville, A. M. Dynamic Structural Biology Experiments at XFEL or Synchrotron Sources. *Methods Mol. Biol.* **2021**, *2305*, 203−228.
(90) Bergmann, U.; Kern, J.; Schoenlein, R. W.; Wernet, P.; Yachandra, V. K.; Yano, J. Using X-ray free-electron lasers for spectroscopy of molecular catalysts and metalloenzymes. *Nat. Rev. Phys.* **2021**, *3* (4), 264−282.
(91) Barends, T. R. M.; Stauch, B.; Cherezov, V.; Schlichting, I. Serial femtosecond crystallography. *Nat. Rev. Methods Primers* **2022**, *2*, 59.
(92) Worrall, J. A. R.; Hough, M. A. Serial femtosecond crystallography approaches to understanding catalysis in iron enzymes. *Curr. Opin. Struct. Biol.* **2022**, *77*, 102486.
(93) Malla, T. N.; Schmidt, M. Transient state measurements on proteins by time-resolved crystallography. *Curr. Opin. Struct. Biol.* **2022**, *74*, 102376.
(94) Brändén, G.; Neutze, R. Advances and challenges in time-resolved macromolecular crystallography. *Science* **2021**, *373*, No. eaba0954.
(95) Schmidt, M. Time-Resolved Macromolecular Crystallography at Modern X-ray Sources. *Methods Mol. Biol.* **2017**, *1607*, 273−294.
(96) Stagno, J. R.; Liu, Y.; Bhandari, Y. R.; Conrad, C. E.; Panja, S.; Swain, M.; Fan, L.; Nelson, G.; Li, C.; Wendel, D. R.; et al. Structures of riboswitch RNA reaction states by mix-and-inject XFEL serial crystallography. *Nature* **2017**, *541*, 242−246.
(97) Kupitz, C.; Olmos, J. L.; Holl, M.; Tremblay, L.; Pande, K.; Pandey, S.; Oberthür, D.; Hunter, M.; Liang, M.; Aquila, A.; et al. Structural enzymology using X-ray free electron lasers. *Struct. Dyn.* **2017**, *4*, 044003.
(98) Mehrabi, P.; Schulz, E. C.; Agthe, M.; Horrell, S.; Bourenkov, G.; et al. Liquid application method for time-resolved analyses by serial synchrotron crystallography. *Nat. Methods* **2019**, *16*, 979−982.
(99) Nomura, T.; Kimura, T.; Kanematsu, Y.; Yamada, D.; Yamashita, K.; Hirata, K.; Ueno, G.; Murakami, H.; Hisano, T.; Yamagiwa, R.; et al. Short-lived intermediate in N(2)O generation by P450 NO reductase captured by time-resolved IR spectroscopy and XFEL crystallography. *Proc. Natl. Acad. Sci. U.S.A.* **2021**, *118* (21), No. e2101481118.
(100) Schmidt, M. Mix and inject, reaction initiation by diffusion for time-resolved macromolecular crystallography. *Adv. Condens. Matter Phys.* **2013**, *2013*, 1−10.
(101) Kurz, S. G.; Bonomo, R. A. Reappraising the use of $\beta$-lactams to treat tuberculosis. *Expert Rev. Anti. Infect. Ther.* **2012**, *10* (9), 999−1006.
(102) Tremblay, L. W.; Fan, F.; Blanchard, J. S. Biochemical and structural characterization of *Mycobacterium tuberculosis* beta-lacta-


https://doi.org/10.1021/acscatal.4c02526
ACS Catal. 2024, 14, 10853−10870

mase with the carbapenems ertapenem and doripenem. *Biochemistry* **2010**, *49*, 3766−3773.
(103) Levine, S. R.; Beatty, K. E. Investigating β-Lactam Drug Targets in *Mycobacterium tuberculosis* Using Chemical Probes. *ACS Infect. Dis.* **2021**, *7* (2), 461−470.
(104) Olmos, J. L., Jr; Pandey, S.; Martin-Garcia, J. M.; Calvey, G.; Katz, A.; Knoska, J.; Kupitz, C.; Hunter, M. S.; Liang, M.; Oberthuer, D.; et al. Enzyme intermediates captured "on the fly" by mix-and-inject serial crystallography. *BMC Biol.* **2018**, *16*, 59.
(105) Malla, T. N.; Zielinski, K.; Aldama, L.; Bajt, S.; Feliz, D.; Hayes, B.; Hunter, M.; Kupitz, C.; Lisova, S.; Knoska, J.; et al. Heterogeneity in *M. tuberculosis* β-lactamase inhibition by Sulbactam. *Nat. Commun.* **2023**, *14* (1), 5507.
(106) Schmidt, M. Practical considerations for the analysis of time-resolved X-ray data. *Struct. Dyn.* **2023**, *10* (4), 044303.
(107) Richter, O. M.; Ludwig, B. Cytochrome *c* oxidase-structure, function, and physiology of a redox-driven molecular machine. *Rev. Physiol. Biochem. Pharmacol.* **2003**, *147*, 47−74.
(108) Michel, H.; Behr, J.; Harrenga, A.; Kannt, A. Cytochrome *c* oxidase: structure and spectroscopy. *Annu. Rev. Biophys. Biomol. Struct.* **1998**, *27*, 329−356.
(109) Ishigami, I.; Sierra, R. G.; Su, Z.; Peck, A.; Wang, C.; Poitevin, F.; Lisova, S.; Hayes, B.; Moss, F. R.; Boutet, S.; Sublett, R. E.; Yoon, C. H.; Yeh, S.-R.; Rousseau, D. L. Structural insights into functional properties of the oxidized form of cytochrome *c* oxidase. *Nat. Commun.* **2023**, *14* (1), 5752.
(110) Freeman, S. L.; Martel, A.; Raven, E. L.; Roberts, G. C. K. Orchestrated Domain Movement in Catalysis by Cytochrome P450 Reductase. *Sci. Rep.* **2017**, *7* (1), 9741.
(111) Klinman, J. P. Dynamically achieved active site precision in enzyme catalysis. *Acc. Chem. Res.* **2015**, *48* (2), 449−56.
(112) Nguyen, R. C.; Davis, I.; Dasgupta, M.; Wang, Y.; Simon, P. S.; Butryn, A.; Makita, H.; Bogacz, I.; Dornevil, K.; Aller, P.; et al. In Situ Structural Observation of a Substrate- and Peroxide-Bound High-Spin Ferric-Hydroperoxo Intermediate in the P450 Enzyme CYP121. *J. Am. Chem. Soc.* **2023**, *145*, 25120.
(113) Gibson, Q. H. Stopped-flow apparatus for the study of rapid reactions. *Discuss. Faraday Soc.* **1954**, *17*, 137.
(114) Biro, F. N.; Zhai, J.; Doucette, C. W.; Hingorani, M. M. Application of stopped-flow kinetics methods to investigate the mechanism of action of a DNA repair protein. *J. Vis. Exp.* **2010**, *37*, 1874.
(115) Hartwell, S. K.; Grudpan, K. Flow-based systems for rapid and high-precision enzyme kinetics studies. *J. Anal. Methods Chem.* **2012**, *2012*, 450716.
(116) Candotti, M.; Orozco, M. The Differential Response of Proteins to Macromolecular Crowding. *PLoS Comput. Biol.* **2016**, *12* (7), No. e1005040.
(117) Senske, M.; Törk, L.; Born, B.; Havenith, M.; Herrmann, C.; Ebbinghaus, S. Protein stabilization by macromolecular crowding through enthalpy rather than entropy. *J. Am. Chem. Soc.* **2014**, *136* (25), 9036−9041.
(118) Hinzpeter, F.; Tostevin, F.; Buchner, A.; Gerland, U. Trade-offs and design principles in the spatial organization of catalytic particles. *Nat. Phys.* **2022**, *18*, 203−211.
(119) Ma, B.; Nussinov, R. Structured crowding and its effects on enzyme catalysis. *Top. Curr. Chem.* **2013**, *337*, 123−137.
(120) Schlichting, I.; Goody, R. S. Triggering methods in crystallographic enzyme kinetics. *Methods Enzymol.* **1997**, *277*, 467−90.
(121) Calvey, G. D.; Katz, A. M.; Schaffer, C. B.; Pollack, L. Mixing injector enables time-resolved crystallography with high hit rate at X-ray free electron lasers. *Struct. Dyn.* **2016**, *3*, 054301.
(122) Calvey, G. D.; Katz, A. M.; Pollack, L. Microfluidic Mixing Injector Holder Enables Routine Structural Enzymology Measurements with Mix-and-Inject Serial Crystallography Using X-ray Free Electron Lasers. *Anal. Chem.* **2019**, *91*, 7139−7144.
(123) Vakili, M.; Han, H.; Schmidt, C.; Wrona, A.; Kloos, M.; de Diego, I.; Dörner, K.; Geng, T.; Kim, C.; Koua, F. H. M.; et al. Mix-and-extrude: high-viscosity sample injection toward time-resolved protein crystallography. *J. Appl. Crystallogr.* **2023**, *56* (4), 1038−1045.
(124) Cha, S. A simple method for derivation of rate equations for enzyme-catalyzed reactions under the rapid equilibrium assumption or combined assumptions of equilibrium and steady state. *J. Biol. Chem.* **1968**, *243* (4), 820−825.
(125) Cleland, W. W. Derivation of rate equations for multisite ping-pong mechanisms with ping-pong reactions at one or more sites. *J. Biol. Chem.* **1973**, *248* (24), 8353−8355.
(126) Kong, M.; Zhang, Y.; Li, Q.; Dong, R.; Gao, H. Kinetics of Horseradish Peroxidase-Catalyzed Nitration of Phenol in a Biphasic System. *J. Microbiol. Biotechnol.* **2017**, *27* (2), 297−305.
(127) Moody, P. C. E.; Raven, E. L. The Nature and Reactivity of Ferryl Heme in Compounds I and II. *Acc. Chem. Res.* **2018**, *51* (2), 427−435.
(128) Lučić, M.; Wilson, M. T.; Svistunenko, D. A.; Owen, R. L.; Hough, M. A.; Worrall, J. A. R. Aspartate or arginine? Validated redox state X-ray structures elucidate mechanistic subtleties of $Fe^{IV}$ = O formation in bacterial dye-decolorizing peroxidases. *J. Biol. Inorg. Chem.* **2021**, *26* (7), 743−761.
(129) Lučić, M.; Svistunenko, D. A.; Wilson, M. T.; Chaplin, A. K.; Davy, B.; Ebrahim, A.; Axford, D.; Tosha, T.; Sugimoto, H.; Owada, S.; et al. Serial Femtosecond Zero Dose Crystallography Captures a Water-Free Distal Heme Site in a Dye-Decolorizing Peroxidase to Reveal a Catalytic Role for an Arginine in FeIV = O Formation. *Angew. Chem., Int. Ed. Engl.* **2020**, *59* (48), 21656−21662.
(130) Lučić, M.; Wilson, M. T.; Tosha, T.; Sugimoto, H.; Shilova, A.; Axford, D.; Owen, R. L.; Hough, M. A.; Worrall, J. A. R. Serial Femtosecond Crystallography Reveals the Role of Water in the One- or Two-Electron Redox Chemistry of Compound I in the Catalytic Cycle of the B-Type Dye-Decolorizing Peroxidase DtpB. *ACS Catal.* **2022**, *12* (21), 13349−13359.
(131) Chen, C.; Shrestha, R.; Jia, K.; Gao, P. F.; Geisbrecht, B. V.; Bossmann, S. H.; Shi, J.; Li, P. Characterization of Dye-decolorizing Peroxidase (DyP) from *Thermomonospora curvata* Reveals Unique Catalytic Properties of A-type DyPs. *J. Biol. Chem.* **2015**, *290*, 23447−23463.
(132) Moreno-Chicano, T.; Carey, L. M.; Axford, D.; Beale, J. H.; Doak, R. B.; Duyvesteyn, H. M. E.; Ebrahim, A.; Henning, R. W.; Monteiro, D. C. F.; Myles, D. A.; et al. Complementarity of neutron, XFEL and synchrotron crystallography for defining the structures of metalloenzymes at room temperature. *IUCrJ.* **2022**, *9* (5), 610−624.
(133) Gumiero, A.; Metcalfe, C. L.; Pearson, A. R.; Raven, E. L.; Moody, P. C. Nature of the ferryl heme in compounds I and II. *J. Biol. Chem.* **2011**, *286* (2), 1260−1268.
(134) Kwon, H.; Schrader, T. E.; Ostermann, A.; Blakeley, M. P.; Raven, E. L.; Moody, P. C. E. Heme peroxidase-trapping intermediates by cryo neutron crystallography. *Methods Enzymol.* **2020**, *634*, 379−389.
(135) Schmidt, M. Time-resolved macromolecular crystallography at pulsed X-ray sources. *Int. J. Mol. Sci.* **2019**, *20*, 1401.
(136) Srajer, V.; Schmidt, M. Watching proteins function with time-resolved X-ray crystallography. *J. Phys. D Appl. Phys.* **2017**, *50*, 373001.
(137) Coquelle, N.; Brewster, A. S.; Kapp, U.; Shilova, A.; Weinhausen, B.; Burghammer, M.; Colletier, J. P. Raster-scanning serial protein crystallography using micro- and nanofocused synchrotron beams. *Acta Crystallogr. D Biol. Crystallogr.* **2015**, *71* (5), 1184−1196.
(138) Hadjidemetriou, K.; Coquelle, N.; Barends, T. R. M.; De Zitter, E.; Schlichting, I.; Colletier, J. P.; Weik, M. Time-resolved serial femtosecond crystallography on fatty-acid photodecarboxylase: lessons learned. *Acta Crystallogr. D Struct. Biol.* **2022**, *78* (9), 1131−1142.
(139) White, W. E.; Robert, A.; Dunne, M. The Linac Coherent Light Source. *J. Synchrotron. Radiat.* **2015**, *22* (3), 472−476.
(140) Ishikawa, T.; Aoyagi, H.; Asaka, T.; Asano, Y.; Azumi, N.; Bizen, T.; Ego, H.; Fukami, K.; Fukui, T.; Furukawa, Y.; et al. A


https://doi.org/10.1021/acscatal.4c02526
ACS Catal. 2024, 14, 10853−10870

compact X-ray free-electron laser emitting in the subångström region. *Nat. Photonics* **2012**, *6*, 540−544.
(141) Kang, H. S.; Min, C. K.; Heo, H.; Kim, C.; Yang, H.; Kim, G.; Nam, I.; Baek, S. Y.; Choi, H.-J.; Mun, G.; et al. Hard X-ray free-electron laser with femtosecond-scale timing jitter. *Nat. Photonics* **2017**, *11*, 708−713.
(142) Ko, I. S.; Kang, H.-S.; Heo, H.; Kim, C.; Kim, G.; Min, C.-K.; Yang, H.; Baek, S. Y.; Choi, H.-J.; Mun, G.; et al. Construction and Commissioning of PAL-XFEL Facility. *Appl. Sci.* **2017**, *7*, 479.
(143) Prat, E.; Abela, R.; Aiba, M.; Alarcon, A.; Alex, J.; Arbelo, Y.; Arrell, C.; Arsov, V.; Bacellar, C.; Beard, C.; et al. A compact and cost-effective hard X-ray free-electron laser driven by a high-brightness and low-energy electron beam. *Nat. Photonics* **2020**, *14*, 748−754.
(144) Decking, W.; Abeghyan, S.; Abramian, P.; Abramsky, A.; Aguirre, A.; Albrecht, C.; Alou, P.; Altarelli, M.; Altmann, P.; Ayman, K.; et al. A MHz-repetition-rate hard X-ray free-electron laser driven by a superconducting linear accelerator. *Nat. Photonics* **2020**, *14*, 391−397.
(145) Altarelli, M.; Mancuso, A. P. Structural biology at the European X-ray free-electron laser facility. *Philos. Trans. R. Soc. London B Biol. Sci.* **2014**, *369* (1647), 20130311.
(146) Grünbein, M. L.; Bielecki, J.; Gorel, A.; Stricker, M.; Bean, R.; Cammarata, M.; Dörner, K.; Fröhlich, L.; Hartmann, E.; Hauf, S.; et al. Megahertz data collection from protein microcrystals at an X-ray free-electron laser. *Nat. Commun.* **2018**, *9* (1), 3487.
(147) Butryn, A.; Simon, P. S.; Aller, P.; Hinchliffe, P.; Massad, R. N.; Leen, G.; Tooke, C. L.; Bogacz, I.; Kim, I. S.; Bhowmick, A.; et al. An on-demand, drop-on-drop method for studying enzyme catalysis by serial crystallography. *Nat. Commun.* **2021**, *12* (1), 4461.
(148) Mehrabi, P.; Sung, S.; von Stetten, D.; Prester, A.; Hatton, C. E.; Kleine-Döpke, S.; Berkes, A.; Gore, G.; Leimkohl, J. P.; Schikora, H.; et al. Millisecond cryo-trapping by the spitrobot crystal plunger simplifies time-resolved crystallography. *Nat. Commun.* **2023**, *14* (1), 2365.
(149) Holmes, S.; Kirkwood, H. J.; Bean, R.; Giewekemeyer, K.; Martin, A. V.; Hadian-Jazi, M.; Wiedorn, M. O.; Oberthür, D.; Marman, H.; Adriano, L.; et al. Megahertz pulse trains enable multihit serial femtosecond crystallography experiments at X-ray free electron lasers. *Nat. Commun.* **2022**, *13* (1), 4708.
(150) Sugahara, M.; Mizohata, E.; Nango, E.; Suzuki, M.; Tanaka, T.; Masuda, T.; Tanaka, R.; Shimamura, T.; Tanaka, Y.; Suno, C.; Ihara, K.; Pan, D.; Kakinouchi, K.; Sugiyama, S.; Murata, M.; Inoue, T.; Tono, K.; Song, C.; Park, J.; Kameshima, T.; Hatsui, T.; Joti, Y.; Yabashi, M.; Iwata, S. Grease matrix as a versatile carrier of proteins for serial crystallography. *Nat. Methods* **2015**, *12*, 61−63.
(151) Botha, S.; Nass, K.; Barends, T. R. M.; Kabsch, W.; Latz, B.; Dworkowski, F.; Foucar, L.; Panepucci, E.; Wang, M. T.; Shoeman, R. L.; et al. Room-temperature serial crystallography at synchrotron X-ray sources using slowly flowing free-standing high-viscosity microstreams. *Acta Crystallogr. D Biol. Crystallogr.* **2015**, *71*, 387−397.
(152) Sugahara, M.; Song, C. Y.; Suzuki, M.; Masuda, T.; Inoue, S.; Nakane, T.; Yumoto, F.; Nango, E.; Tanaka, R.; Tono, K.; et al. Oil-free hyaluronic acid matrix for serial femtosecond crystallography. *Sci. Rep.* **2016**, *6*, 24484.
(153) Conrad, C. E.; Basu, S.; James, D.; Wang, D. J.; Schaffer, A.; Roy-Chowdhury, S.; Zatsepin, N. A.; Aquila, A.; Coe, J.; Gati, C.; et al. A novel inert crystal delivery medium for serial femtosecond crystallography. *IUCrJ.* **2015**, *2*, 421−430.
(154) Sugahara, M.; Nakane, T.; Masuda, T.; Suzuki, M.; Inoue, S.; Song, C. Y.; Tanaka, R.; Nakatsu, T.; Mizohata, E.; Yumoto, F.; et al. Hydroxyethyl cellulose matrix applied to serial crystallography. *Sci. Rep.* **2017**, *7*, 703.
(155) Nam, K. H. Lard injection matrix for serial crystallography. *Int. J. Mol. Sci.* **2020**, *21*, 5977.
(156) Mariani, V.; Morgan, A.; Yoon, C. H.; Lane, T. J.; White, T. A.; O'Grady, C.; Kuhn, M.; Aplin, S.; Koglin, J.; Barty, A.; Chapman, H. N. *OnDA*: online data analysis and feedback for serial X-ray imaging. *J. Appl. Crystallogr.* **2016**, *49* (3), 1073−1080.
(157) White, T. A.; Barty, A.; Stellato, F.; Holton, J. M.; Kirian, R. A.; Zatsepin, N. A.; Chapman, H. Crystallographic data processing for free-electron laser sources. *Acta Crystallogr. Sec. D Struct. Biol.* **2013**, *69*, 1231−1240.
(158) White, T. A.; Mariani, V.; Brehm, W.; Yefanov, O.; Barty, A.; Beyerlein, K. R.; Chervinskii, F.; Galli, L.; Gati, C.; Nakane, T.; et al. Recent developments in CrystFEL. *J. Appl. Crystallogr.* **2016**, *49*, 680−689.
(159) Barty, A.; Kirian, R. A.; Maia, F. R. N. C.; Hantke, M.; Yoon, C. H.; White, T. A.; Chapman, H. Cheetah: Software for high-throughput reduction and analysis of serial femtosecond X-ray diffraction data. *J. Appl. Crystallogr.* **2014**, *47* (3), 1118−1131.
(160) Hattne, J.; Echols, N.; Tran, R.; Kern, J.; Gildea, R. J.; Brewster, A. S.; Alonso-Mori, R.; Glöckner, C.; Hellmich, J.; Laksmono, H.; et al. Accurate macromolecular structures using minimal measurements from X-ray free-electron lasers. *Nat. Methods* **2014**, *11*, 545−548.
(161) Kabsch, W. Processing of X-ray snapshots from crystals in random orientations. *Acta Crystallographica Sect. D Struct. Biol.* **2014**, *70*, 2204−2216.
(162) Ginn, H. M.; Evans, G.; Sauter, N. K.; Stuart, D. I. On the release of cppxfel for processing X-ray free-electron laser images. *J. Appl. Crystallogr.* **2016**, *49*, 1065−1072.
(163) Shin, H.; Kim, S.; Yoon, C. H. Data Analysis using Psocake at PAL-XFEL. *J. Korean Phys. Soc.* **2018**, *73*, 16−20.
(164) Nakane, T.; Joti, Y.; Tono, K.; Yabashi, M.; Nango, E.; Iwata, S.; Ishitani, R.; Nureki, O. Data processing pipeline for serial femtosecond crystallography at SACLA. *J. Appl. Crystallogr.* **2016**, *49*, 1035−1041.
(165) Turkot, O.; Dall'Antonia, F.; Bean, R. J.; E, J.; Fangohr, H.; Ferreira de Lima, D. E.; Kantamneni, S.; Kirkwood, H.; Koua, F. H. M.; Mancuso, A. P.; et al. Toward automated analysis of serial crystallography data at the European XFEL. *Proc. SPIE* **2023**, *13*, 12581 X-ray Free-Electron Lasers: Advances in Source Development and Instrumentation VI, 125810M (9 June 2023).
(166) Turkot, O.; Dall'Antonia, F.; Bean, R. J.; E, J.; Fangohr, H.; Ferreira de Lima, D. E.; Kantamneni, S.; Kirkwood, H. J.; Koua, F. H. M.; Mancuso, A. P.; et al. EXtra-Xwiz: A Tool to Streamline Serial Femtosecond Crystallography Workflows at European XFEL. *Crystals* **2023**, *13*, 1533.
(167) Tenboer, J.; Basu, S.; Zatsepin, N.; Pande, K.; Milathianaki, D.; Frank, M.; Hunter, M.; Boutet, S.; Williams, G. J.; Koglin, J. E.; et al. Time-resolved serial crystallography captures high-resolution intermediates of photoactive yellow protein. *Science* **2014**, *346* (6214), 1242−1246.
(168) Pande, K.; Hutchison, C. D.; Groenhof, G.; Aquila, A.; Robinson, J. S.; Tenboer, J.; Basu, S.; Boutet, S.; DePonte, D. P.; Liang, M.; et al. Femtosecond structural dynamics drives the trans/cis isomerization in photoactive yellow protein. *Science* **2016**, *352* (6286), 725−729.
(169) Steinfeld, J. I.; Francisco, J. S.; Hase, W. L. *Chemical Kinetics and Dynamics*. 1989, Prentice Hall, NJ.
(170) Schmidt, M.; Rajagopal, S.; Ren, Z.; Moffat, K. Application of singular value decomposition to the analysis of time-resolved macromolecular X-ray data. *Biophys. J.* **2003**, *84*, 2112−2129.
(171) Rajagopal, S.; Schmidt, M.; Anderson, S.; Ihee, H.; Moffat, K. Analysis of experimental time-resolved crystallographic data by singular value decomposition. *Acta Crystallogr. D Biol. Crystallogr.* **2004**, *60* (5), 860−871.
(172) Ihee, H.; Rajagopal, S.; Srajer, V.; Pahl, R.; Anderson, S.; Schmidt, M.; Schotte, F.; Anfinrud, P. A.; Wulff, M.; Moffat, K. Visualizing reaction pathways in photoactive yellow protein from nanoseconds to seconds. *Proc. Natl. Acad. Sci. U.S.A.* **2005**, *102* (20), 7145−7150.
(173) Zapata, A. L.; Kumar, M. R.; Pervitsky, D.; Farmer, P. J. A singular value decomposition approach for kinetic analysis of reactions of HNO with myoglobin. *J. Inorg. Biochem.* **2013**, *118*, 171−178.


https://doi.org/10.1021/acscatal.4c02526
*ACS Catal.* 2024, 14, 10853−10870

(174) Koshland, D. E., Jr Application of a theory of enzyme specificity to protein synthesis. *Proc. Natl. Acad. Sci. USA* **1958**, *44*, 98−104.
(175) De Zitter, E.; Coquelle, N.; Oeser, P.; Barends, T. R. M.; Colletier, J. P. Xtrapol8 enables automatic elucidation of low-occupancy intermediate-states in crystallographic studies. *Commun. Biol.* **2022**, *5* (1), 640.
(176) Li, H.; Nakajima, Y.; Nango, E.; Owada, S.; Yamada, D.; Hashimoto, K.; Luo, F.; Tanaka, R.; Akita, F.; Kato, K.; Kang, J.; Saitoh, Y.; Kishi, S.; Yu, H.; Matsubara, N.; Fujii, H.; Sugahara, M.; Suzuki, M.; Masuda, T.; Kimura, T.; Thao, T. N.; Yonekura, S.; Yu, L.-J.; Tosha, T.; Tono, K.; Joti, Y.; Hatsui, T.; Yabashi, M.; Kubo, M.; Iwata, S.; Isobe, H.; Yamaguchi, K.; Suga, M.; Shen, J.-R. Oxygen-evolving photosystem II structures during S1-S2-S3 transitions. *Nature* **2024**, *626*, 670−677.
(177) Bhowmick, A.; Hussein, R.; Bogacz, I.; Simon, P. S.; Ibrahim, M.; et al. Structural evidence for intermediates during $O_2$ formation in photosystem II. *Nature* **2023**, *617*, 629−636.
(178) Maestre-Reyna, M.; Wang, P. H.; Nango, E.; Hosokawa, Y.; Saft, M.; et al. Visualizing the DNA repair process by a photolyase at atomic resolution. *Science* **2023**, *382*, No. eadd7795.
(179) Christou, N.-E.; Apostolopoulou, V.; Melo, D. V. M.; Ruppert, M.; Fadini, A.; et al. Time-resolved crystallography captures light-driven DNA repair. *Science* **2023**, *382*, 1015−1020.
(180) Nango, E.; Royant, A.; Kubo, M.; Nakane, T.; Wickstrand, C.; et al. A three-dimensional movie of structural changes in bacteriorhodopsin. *Science* **2016**, *354*, 1552−1557.
(181) Skopintsev, P.; Ehrenberg, D.; Weinert, T.; James, D.; Kar, R. K.; Johnson, P. J. M.; Ozerov, D.; Furrer, A.; Martiel, I.; Dworkowski, F.; Nass, K.; Knopp, G.; Cirelli, C.; Arrell, C.; Gashi, D.; Mous, S.; Wranik, M.; Gruhl, T.; Kekilli, D.; Brunle, S.; Deupi, X.; Schertler, G. F. X.; Benoit, R. M.; Panneels, V.; Nogly, P.; Schapiro, I.; Milne, C.; Heberle, J.; Standfuss, J. Femtosecond-to-millisecond structural changes in a light-driven sodium pump. *Nature* **2020**, *583*, 314−318.
(182) Gruhl, T.; Weinert, T.; Rodrigues, M. J.; Milne, C. J.; Ortolani, G.; et al. Ultrafast structural changes direct the first molecular events of vision. *Nature* **2023**, *615*, 939−944.
(183) Livesay, D. R. *Protein Dynamics; Methods in Molecular Biology*; Humana: Totowa, NJ, 2014. DOI: 10.1007/978-1-62703-658-0.
(184) Neutze, R. Opportunities and challenges for time-resolved studies of protein structural dynamics at X-ray free-electron lasers. *Philos. Trans. R. Soc. B* **2014**, *369*, 20130318.
(185) Vidossich, P.; De Vivo, M. The role of first principles simulations in studying (bio)catalytic processes. *Chem. Catalysis* **2021**, *1*, 69−87.
(186) Sikorski, M.; Ramilli, M.; de Wijn, R.; Hinger, V.; Mozzanica, A.; et al. First operation of the JUNGFRAU detector in 16-memory cell mode at European XFEL. *Front. Phys.* **2023**, *11*, 1303247.
(187) Mous, S.; Poitevin, F.; Hunter, M. S.; Asthagiri, D. N.; Beck, T. L. Structural biology in the age of X-ray free-electron lasers and exascale computing. *Curr. Opin. Struct. Biol.* **2024**, *86*, 102808.
(188) Klyshko, E.; Kim, J. S.-H.; McGough, L.; Valeeva, V.; Lee, E.; Ranganathan, R.; Rauscher, S. Functional protein dynamics in a crystal. *Nat. Commun.* **2024**, *15*, 3244.
(189) Clinger, J. A.; Moreau, D. W.; McLeod, M. J.; Holyoak, T.; Thorne, R. E. Millisecond mix-and-quench crystallography (MMQX) enables time-resolved studies of PEPCK with remote data collection. *IUCrJ.* **2021**, *8* (5), 784−792.
(190) Stubbs, J.; Hornsey, T.; Hanrahan, N.; Esteban, L. B.; Bolton, R.; et al. Droplet microfluidics for time-resolved serial crystallography. *IUCrJ.* **2024**, *11* (2), 237−248.
(191) Bar-Even, A.; Noor, E.; Savir, Y.; Liebermeister, W.; Davidi, D.; et al. The moderately efficient enzyme: evolutionary and physicochemical trends shaping enzyme parameters. *Biochemistry* **2011**, *50*, 4402−4410.


https://doi.org/10.1021/acscatal.4c02526
*ACS Catal.* 2024, 14, 10853−10870